frontiers in Earth Science

ORIGINAL RESEARCH
published: 26 November 2021
doi: 10.3389/feart.2021.766946

Depositional Model for Turbidite Lobes in Complex Slope Settings Along Transform Margins: The Motta San Giovanni Formation (Miocene—Calabria, Italy)

Sébastien Rohais[1], Julien Bailleul[2], Sandra Brocheray[2], Julien Schmitz[1], Paolo Paron[3], Francis Kezirian[4] and Pascal Barrier[2]*

[1]IFP Energies Nouvelles, Rueil-Malmaison, France, [2]U2R 7511, Basins-Reservoirs-Resources (B2R), Geosciences Department, UniLaSalle - University of Picardie Jules Verne, Beauvais, France, [3]HE Delft, Institute for Water Education, Delft, Netherlands, [4]MARBREK-CMF, Etrochey, France

OPEN ACCESS

Edited by:
Rosanna Maniscalco, University of Catania, Italy

Reviewed by:
Salvatore Critelli, University of Calabria, Italy
Yvonne Therese Spychala, Leibniz University Hannover, Germany

***Correspondence:**
Sébastien Rohais
sebastien.rohais@ifpen.fr

Specialty section:
This article was submitted to Sedimentology, Stratigraphy and Diagenesis, a section of the journal Frontiers in Earth Science

Received: *30 August 2021*
Accepted: *11 October 2021*
Published: *26 November 2021*

Citation:
Rohais S, Bailleul J, Brocheray S, Schmitz J, Paron P, Kezirian F and Barrier P (2021) Depositional Model for Turbidite Lobes in Complex Slope Settings Along Transform Margins: The Motta San Giovanni Formation (Miocene—Calabria, Italy). Front. Earth Sci. 9:766946. doi: 10.3389/feart.2021.766946

Intraslope lobes, or perched lobes, are attracting scientific interest because they represent a key archive between the shelf and the deep basin plain when looking at a complete source-to-sink depositional system across a continental margin and can form significant offshore hydrocarbon plays. In this study, we focus on a detailed characterization of intraslope lobes of the Motta San Giovanni Formation (Miocene, Calabria), which were deposited in confined conditions during the Miocene along a transform margin. We determine the typical facies associations and stratigraphic architecture of these intraslope lobes using a 3D digital outcrop model resulting from a combined Uncrewed Aerial Vehicle (UAV) and walking acquisition, together with sedimentological logging and geological mapping. We propose recognition criteria for the identification of intraslope lobes, including facies and geometries, integrated within a depositional model. A comparison with other well-known intraslope and confined lobes, as well as basin floor lobes, is finally discussed, to highlight the peculiarities of intraslope lobes deposited along transform margins. The diagnostic depositional model for these types of intraslope lobes includes four main stages of evolution: *1*) Stage 1—isolated detached lobe precursor in response to a flushed hydraulic jump, *2*) Stage 2—prograding and aggrading lobe elements associated with a relatively stable and submerged hydraulic jump in the Channel-Lobe Transition Zone (CLTZ), *3*) Stage 3—major bypass associated with lateral accretion and local aggradation interpreted as a renewal of a normal hydraulic jump in the CTLZ, and *4*) Stage 4—erosion and bypass then abandonment. The development of intraslope lobes along active transform margins is allowed by tectonically induced slope segmentation and local confinement. In such a context, flow stripping and overspill processes occurred. Resulting lobes appear to be particularly small and relatively thin sandy deposits. They could be considered end-member in a lobe classification based on the Net-to-Gross content (high) and taking into account their thickness/width ratio (intermediate between 10:1 and 100:1 lines).

Keywords: turbidites, lobe deposits, intraslope, bypass, transform margin, miocene, UAV, uncrewed aerial vehicle

INTRODUCTION

Intraslope lobes, or perched lobes (Plink-Björklund and Steel, 2002), are attracting scientific interest because they represent a key archive between the shelf and the deep basin plain when looking at a complete source-to-sink depositional system across a continental margin, and can form significant offshore hydrocarbon plays. Key subsurface studies include the Brazilian Campos basin (Albertão et al., 2011), the Niger Delta slope (Adeogba et al., 2005; Prather et al., 2012; Zhang et al., 2016; Jobe et al., 2017), the Lower Congo Basin, offshore Angola (Oluboyo et al., 2014; Picot et al., 2016; Dennielou et al., 2017), or the Gulf of Mexico (e.g. Holman and Robertson, 1994; McGee et al., 1994; Prather et al., 1998; Fiduk et al., 1999; Booth et al., 2003; 2012; Pirmez et al., 2012). Sedimentary processes and stratigraphic architecture were addressed in several examples including the Gioia Basin, southeastern Tyrrhenian Sea (Gamberi et al., 2011; Gamberi and Rovere, 2011), the Algarve Margin, offshore Portugal (Marchès et al., 2010) for modern seabed studies, and the Karoo basin, South Africa (Spychala et al., 2015), the Pab system, Pakistan (Eschard et al., 2004), and the Baiyun Sag, South China Sea (Li et al., 2012) for ancient exhumed studies.

These perched lobes are also described as confined lobes, of which an important literature is available from outcrop, with for example the world class Annot Sandstones, France (Joseph et al., 2000; Guillocheau et al., 2004; Joseph and Lomas, 2004; Mulder et al., 2010; Etienne et al., 2012), the Sorbas basin, Spain (Kleverlaan, 1989; Postma and Kleverlaan, 2018) or the Hikurangi margin, New Zealand (Burgreen and Graham, 2014; McArthur et al., 2021), and from modern system such as the Golo system, East Corsica (Gervais et al., 2004, 2006; Deptuck et al., 2008).

These lobes have common characteristics: *1*) they display a smaller lateral extent and lower aspect ratio than their basin floor counterparts (Plink-Björklund and Steel, 2002; Deptuck et al., 2008; Postma and Kleverlaan, 2018), *2*) they exhibit an overall mounded convex-up geometry in radial profile (e.g., Oluboyo et al., 2014), *3*) they show a high proportion of relative coarse and massive sands (i.e. high Net to Gross ratio) (Komar, 1971; Ferry et al., 2005; Postma and Kleverlaan, 2018), *4*) they are found in association with slumps and mass transport complexes (MTCs) (Walker, 1978; Adeogba et al., 2005; Gamberi and Rovere, 2011; Li et al., 2012), and *5*) evidences for incision are frequent (Adeogba et al., 2005; Ferry et al., 2005; Flint et al., 2011; Barton, 2012; Prather et al., 2012). This final characteristic is critical as incision commonly records the bypass of sediment toward the final sink in the basin floor lobes. However, it is still unclear when sediments are exported downdip, especially the coarser material, considering the dynamic and architecture of the intraslope lobes. Guillocheau et al. (2004) proposed a stratigraphic depositional model where the topmost surface of lobe corresponds to a flattened and smooth bypass surface. Postma and Kleverlaan (2018) documented a detailed morphodynamic study to illustrate the main depositional stage of the lobe evolution in response to hydraulic jump dynamic, without addressing large erosions and related bypass processes. Spychala et al. (2015) presented a depositional model with a final incision by a low aspect ratio channel responsible for downdip sediment export. As intraslope lobes do not represent the architectural element located in the most distal part of a turbidite system at the margin scale, understanding their depositional architecture and morphodynamics is key to characterize the record of deep-marine systems and their preserved stratigraphic successions in the abyssal plain. Amongst all tectonic margins, transform margins commonly show topographically complex slopes, and the sediment distribution as well as the geometries of turbidite architectural elements are still poorly known in this context (MacGregor et al., 2003; Pellegrini and Ribeiro, 2018).

In this study, we focus on a detailed characterization of some intraslope lobes of the Motta San Giovanni Formation (Calabria), which were deposited during the Miocene along a transform margin (**Figure 1**). These outcrops spectacularly expose the 3D lobes architecture thanks to rapid Pleistocene uplift, providing a unique opportunity to characterize such a complex sedimentary system along a transform margin. First, we integrate these lobes in a broader regional setting by geological mapping and paleocurrent analysis, allowing their distribution across a slope comprising perched mini-basins to be assessed. Second, we determine the typical facies associations and stratigraphic architecture of these intraslope lobes. Then, we propose recognition criteria for the identification of intraslope lobes through a depositional model. A comparison with other well-known intraslope and confined lobes, as well as basin floor lobes, is also discussed, to highlight the peculiarities of intraslope lobes deposited along transform margins.

MATERIALS AND METHODS

Fieldwork was undertaken to characterize the Miocene turbidites from the Motta San Giovanni Formation outcropping in the southeastern region of Calabria in detail (**Figure 2A**). Geological mapping over a survey area of 14×17 km^2 (ca. 240 km^2) has been carried out to revise the geological maps created there by the IGAL (Institut Géologique Albert-de-Lapparent) groups and followers regularly since 1981 (e.g. Barrier, 1982; Morlo, 1985; Becue, 1988; Gallet de Saint-Aurin, 1988; Bouchet, 1990; Manoux, 1999; Schepers, 1999; Rohais, 2000; Thomaïdis, 2000; Raber, 2003; Vallee, 2003; Guillois and Polard-Taine, 2016; Pichancourt and Terrier, 2016; Colas and Ripoll, 2017; Chirol et al., 2019; Marchiel and Rispal, 2019; Bourel and Degrave, 2020; Guillet de Chatelus and Prosperi, 2020) (**Figure 2A**).

Three areas have been studied in very high resolution for stratigraphic issues: *1*) the Motta area (1×1.5 km^2) located in the vicinity of the Motta San Giovanni town, *2*) the Saetta area located along the Saetta river (0.8×0.8 km^2), and *3*) the Di Leo area (0.7×0.7 km^2) (**Figure 2A**).

Architecture and bed continuity in these areas were mapped by physical tracing in the field with the help of a 3-dimensional outcrop model (Virtuoso@IFPEN, Deschamps et al., 2013, 2017; Schmitz et al., 2014). The dimensions of the lobes were quantified from the 3D models using the Virtuoso interactive tool to

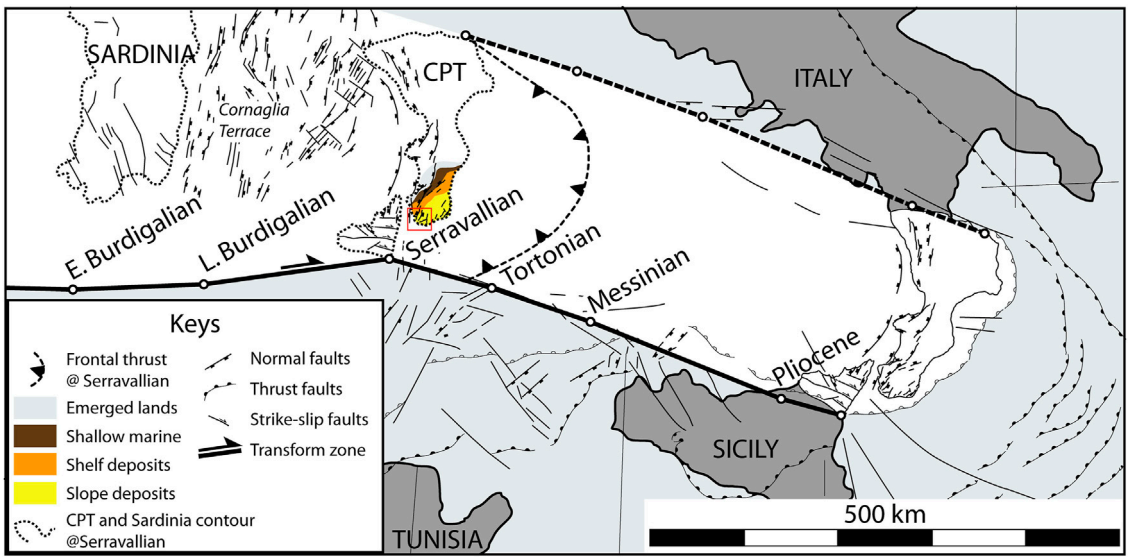

FIGURE 1 | Paleogeographic reconstruction of the Motta San Giovanni Formation during the early Serravallian. Relative position of Sardinia and CPT compared to Italy, Sicily, and Tunisia considered fixe (Gray) based on the reconstruction for the kinematic complex D2 of Vitale and Ciarcia (2013). Relative position of CPT and migration path from Vitale and Ciarcia (2013). Fault pattern is from Leprêtre et al. (2019) and Jolivet et al. (2021) and reference herein. Fault pattern in CPT is refined using Kezirian et al. (1994) (Sicily) and Brutto et al. (2018) (Calabria). Depositional environments are from the synthesis of Raber (2003) and reference herein. Red square illustrates the studied area.

preserve spatial precision and dimensionality. The images (n = 1770, 40 megapixels resolution) were made by land foot acquisition combined with DJI Phantom Vision 2+ drone-attached camera both with a GNSS (Global Navigation Satellite System) positioning system. The quality and resolution (<5 cm) of the 3D models provided adequate resolution for mapping purposes at the bed scale as well as for architectural and facies analysis (**Figure 3**).

A total of 22 sedimentological sections were logged at high resolution (scale: 1:12.5, cumulative total thickness = 176 m). Turbidite facies are interpreted by using the newly proposed facies schemes of Talling et al. (2012) and Postma and Cartigny (2014) for sub- and super-critical turbidity current deposits following the recent work of Postma and Kleverlaan (2018). The Bouma sequence (Bouma, 1962) with five different facies abbreviated as Ta-Te units is used as an overall facies framework, with an expanded version for the Tb unit (Cartigny et al., 2013; Postma and Cartigny, 2014). Paleocurrents directions were acquired from ripples (n = 679), groove marks and channel axis (n = 229) all over the revised geological map.

GEOLOGICAL AND STRATIGRAPHIC SETTINGS

Calabria: A Complex Geodynamic Setting

The Calabria–Peloritani terrane (CPT) is a fault-bounded terrane comprising Calabria, i.e. the region at the southern tip of the Italy, and the Peloritani Mountains of northeastern Sicily (**Figure 1**). The CPT is composed of a pre-Mesozoic crystalline basement with a thin and discontinuous Mesozoic sedimentary cover (Roda, 1965). It shows evidence of pre-Neogene tectonism and metamorphism, in marked contrast with the geology of the adjacent orogenic chains (i.e. the Apennines, including Sicily; Bonardi et al., 2001). Two main geodynamic phases characterize the construction of the CPT (Dewey et al., 1989; Faccenna et al., 2001, Critelli, 2018): *1*) a Late Oligocene–Middle Miocene trench migration, accompanied by opening of the Ligurian–Provençal back-arc basin and *2*) a Tortonian–Pleistocene migration, with opening of the Tyrrhenian back-arc basin. Numerous paleogeographic reconstructions of this part of the Mediterranean region have been proposed (e.g. Boullin et al., 1986; Dercourt et al., 1986; Dewey et al., 1989; Faccenna et al., 2001; Critelli et al., 2011, 2017; Vitale and Ciarcia, 2013; Critelli, 2018; Butler et al., 2020; Romagny et al., 2020; Milia et al., 2021) and controversies that go far beyond the scope of our work still exist. No matter what the paleo-reconstruction was, during Langhian to Messinian (Middle to Late Miocene), the CPT was localized to the NW of present-day Sicily (**Figure 1**), conforming to a transform margin setting *sensu* Type 2a of Wilson (1965). At this time, the southern portion of the CPT was facing a relatively deep basin (Algerian Basin, Sardinia Channel), where normal faults are still preserved to the south of the Cornaglia Terrace presently located to the north of Tunisia and to the west of Sicily (**Figure 1**). Very thick Tortonian deposits are preserved in inverted faulted blocks in the offshore of western Sicily (Milia et al., 2021). The southern margin of the CPT was recently revisited and integrated into the dynamic of the Mediterranean back-arc regions and tear faults (Jolivet et al.,

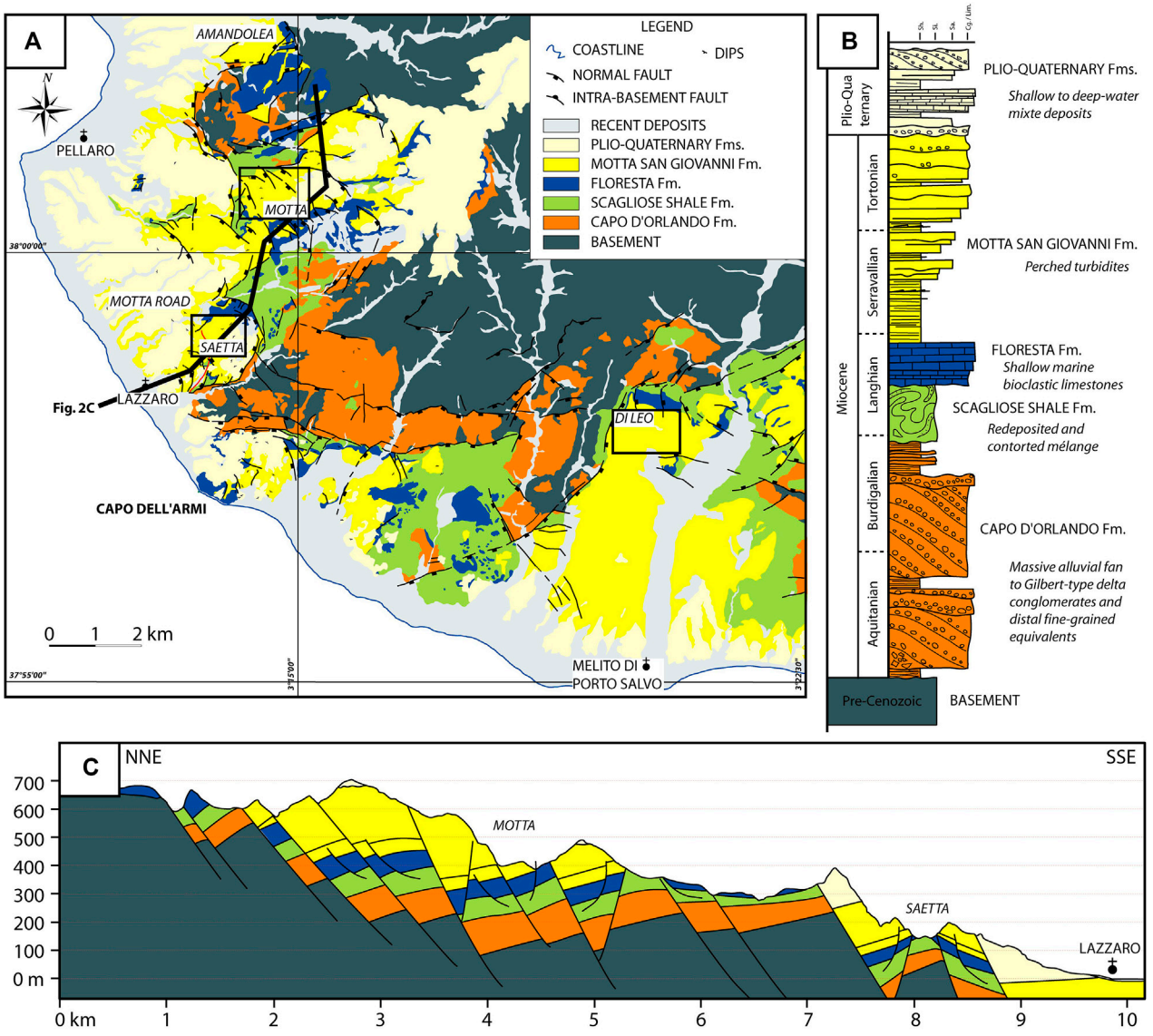

FIGURE 2 | (A) Simplified geological map of the southwestern most part of Calabria. The three areas studied in very high resolution for stratigraphic issues are illustrated with black rectangle. **(B)** Schematic stratigraphic section of the Cenozoic deposits in the southwestern most part of Calabria. Sh., Shale; Si., Siltstone; Sa., Sandstone; Cg./Lim., Conglomerate or Limestone. **(C)** Cross-section illustrating the tilted block and structural pattern in the Motta and Saetta areas. See location on **Figure 2A**.

2021). It is described as a transfer zone: the Catalan-Baleares-Sicily Transfer Zone (CBSTZ). It accommodates the rotation of the Corsica-Sardinia block and the related opening of the southern Tyrrhenian Sea.

Cenozoic Stratigraphy and Structures

In the study area, the Cenozoic stratigraphy is commonly subdivided into several formations (**Figure 2B**). The first deposits are Oligocene (Barrier et al., 1987) to Early Miocene (Aquitanian, Bonardi et al., 1980) in age while the most recent deposits are up to the Pleistocene (Barrier et al., 1987; Tripodi et al., 2013).

At base, the Capo d'Orlando Formation (uppermost Chattian–Burdigalian, Bonardi et al., 1980; Barrier et al., 1987) is a ca. 600-m-thick siliciclastic unit composed of massive conglomerates and laterally equivalent finer-grained deposits. It is organized into a proximal-distal depositional profile ranging from alluvial fans through Gilbert-type deltas, then distal turbidites in a hemipelagic setting (**Figure 2B**).

The Capo d'Orlando Formation is unconformably overlain by the Scagliose shale Formation (Cortese, 1895), informally named "varicolored clays" (**Figure 2B**). It consists of a *mélange* composed of a pelitic, highly sheared matrix enclosing quartz-arenite and limestone–marl blocks (Cavazza et al., 1997). Strontium-isotope ages and foraminiferal biostratigraphy of the underlying and overlying units indicate that the Scagliose shale Formation was emplaced between 17 and 14 Ma (late

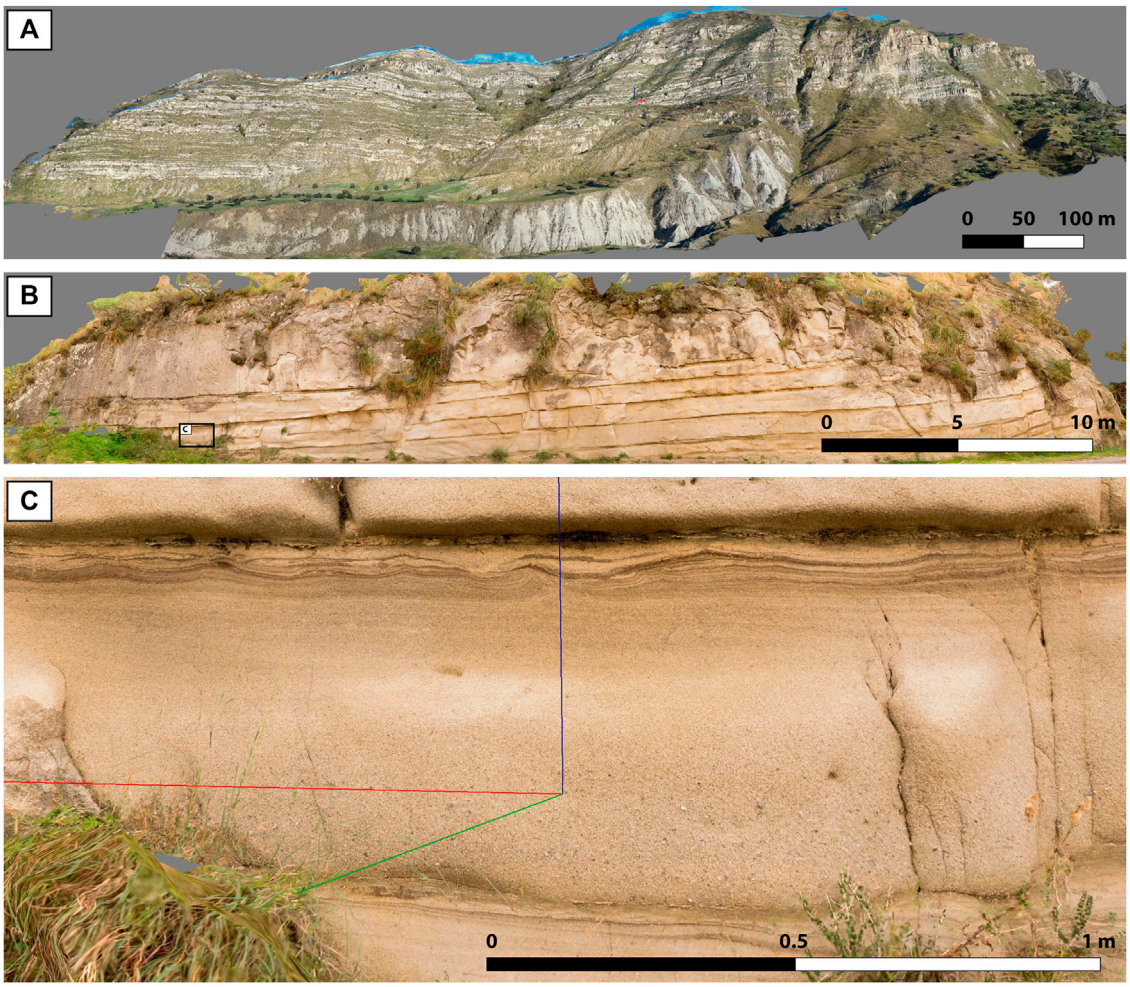

FIGURE 3 | Illustration of the resolution of the 3D drone acquisition dataset (Motta area). The embedded scale used in the present study is presented, from panoramic stratigraphic architectures of the Motta area **(A)**, to bed sets **(B)** and individual beds **(C)**. **Figure 3C** corresponds to the black rectangle on **Figure 3B**.

Burdigalian–Langhian, Bonardi et al., 1980), possibly over a shorter time span (Patterson et al., 1995; Cavazza et al., 1997). According to Cavazza et al. (1997) and Bonardi et al. (2001), the mélange was deposited when the southern edge of the CPT started to collide with the African plate.

The Floresta Formation (Cortese, 1895; Ogniben, 1969) is transgressive on the Scagliose shale Formation, and locally onlaps the Capo d'Orlando Formation and the pre-Cenozoic basement (Barrier et al., 1987). It consists of relatively thin (5–80 m-thick) shallow marine bioclastic mixed limestones (**Figure 2B**), evolving progressively to deeper depositional settings from the north west to the south east.

The Motta San Giovanni Formation (Barrier et al., 1987) is a thick (400–600 m-thick) transgressive unit on the Floresta Formation (**Figure 2B**). It is subdivided into a basal and an upper member, Motta 1 and Motta 2 respectively. They are interpreted to be deposited from density currents in a proximal marine environment, primarily the slope and base of slope (Cavazza et al., 1997; Cavazza and Ingersoll, 2005). The age of the Formation is based on faunal assemblages and ranges from Tortonian, upper Serravallian to lower Messinian (Selli, 1979), to upper Langhian to Tortonian (Barrier et al., 1987).

The Plio-Quaternary deposits include several formations (Barrier et al., 1987) that have recorded major base-level changes (**Figure 2B**). They correspond to mixed deposits, from deep open marine to shallow restricted settings, and show multiple internal unconformities (Barrier et al., 1987; Cavazza et al., 1997). A Pleistocene system of perched marine and fluvial terraces discontinuously overlies older Formations (Barrier et al., 1986; 1987). These terraces are horizontal or subhorizontal and can be found at elevations reaching more than 1,000 m above present-day sea level, thus indicating a dramatic uplift of Calabria during the last 700 ka (Tortorici et al., 1995; Tripodi et al., 2018).

The geological map was revised (**Figure 2A**) highlighting major normal faults with vertical throw of >1000 m and mainly NE-SW orientation (**Figure 2C**). Three main blocks are organized as a succession of piano-like keys dipping

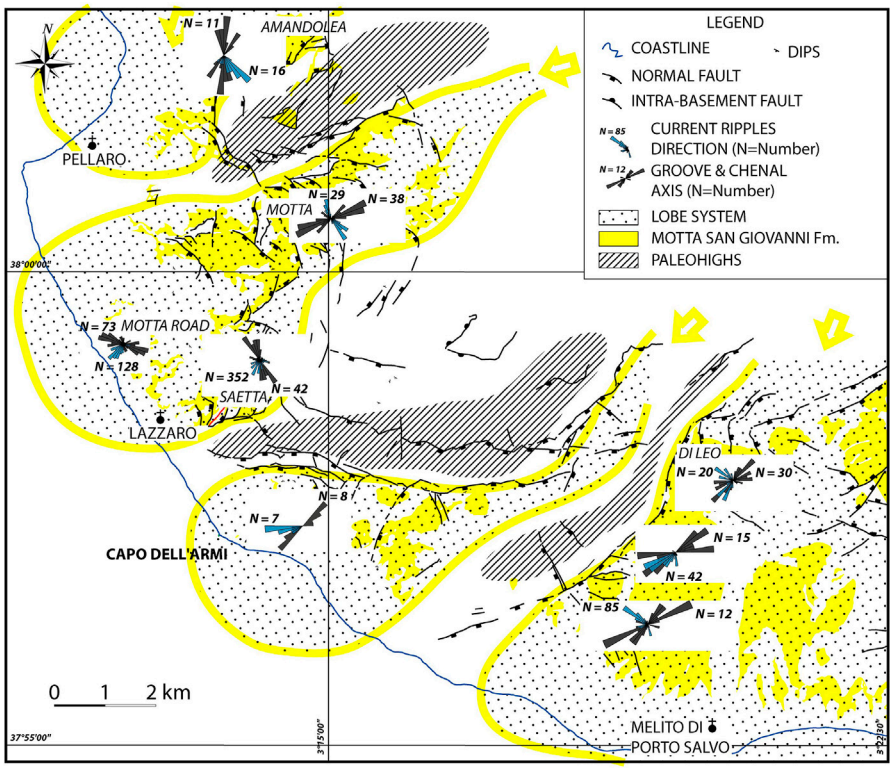

FIGURE 4 | Paleogeographic interpretation and lobe systems of the Motta San Giovanni Formation (Serravallian to Tortonian). Four systems are highlighted from NW to SE, separated by paleohighs corresponding to the crests of early Miocene tilted blocks. Yellow arrows illustrate to sediment supply entry points.

toward the SW: *1*) Amandolea, *2*) Motta-Saetta, and *3*) Di Leo faulted blocks. Each block is affected by superimposed shallow rooted syn-sedimentary normal faults, showing spoon-shape and mainly oriented NW-SE (**Figure 2C**). Major NW-SE normal faults also crosscut the three main blocks and are mainly associated with Plio-pleistocene deformation (Barrier et al., 1987).

Miocene paleocurrents witness the sediment dispersal over the main three tilted blocks. In the Amandolea area, the main axis for the sediment transit is to the south, toward the main fault plan (**Figure 4**). In the Motta area, the main direction is aligned with the main tilted block fault, i.e. NE-SW. In the Saetta and Motta Road area, complex and multiple directions suggest sediment dispersal influenced by local normal faults. In the Di Leo area, the main axis for sediment transport is to the southwest, which is the main tilted block fault direction (**Figure 4**).

Coeval proximal depositional environments of the Motta San Giovanni Formation, including the shallow marine "Clypeaster sandstone" (Barrier et al., 1987; Cavazza et al., 1997), are preserved at north and north-east of the Messina strait (**Figure 1**), providing the opportunity to estimate the distance to the shoreline for the studied outcrops. The Amandolea area is located ca. 14–18 km, the Motta area ca. 24–28 km, the Saetta area ca. 28–32 km, and the Di Leo area ca. 32–36 km offshore the Miocene shoreline. Faunal assemblages indicate a paleobathymetry of ca. 100–300 m in the Motta area and 300–900 m in the Di Leo area (Nicolleau et al.).

FACIES AND ARCHITECTURAL ELEMENTS

The fan lobe terminology developed by Mulder and Etienne (2010) and Gaillot et al. (2015) is followed here, as well as the facies associations and lobe subdivision proposed by Prélat et al. (2009) and Spychala et al. (2015). Facies, facies associations and architectural elements are presented in **Figures 5**–**7**.

Facies Association 1: Channel-Levee (C-Le)

Description

This facies association is dominated by thick-bedded (2–10 m), massive to laminated, very coarse- to medium-grained sandstones, with floating gravels derived from basement rocks (gneiss, granite, micaschists). Layers with fine pebbly gravel to pebble conglomerate are commonly aligned along large-scale sigmoidal cross-stratification, as well as monogenic mud-clast breccias (**Figure 5B**). Large bioturbation (*Ophiomorpha*-like) is often preserved in the upper part of the beds (**Figure 5C**). Coarse- to very-coarse-grained cross-bedded sandstones and pebbly sandstones could be preserved just above the basal erosive surface of the facies association. The basal erosive surface

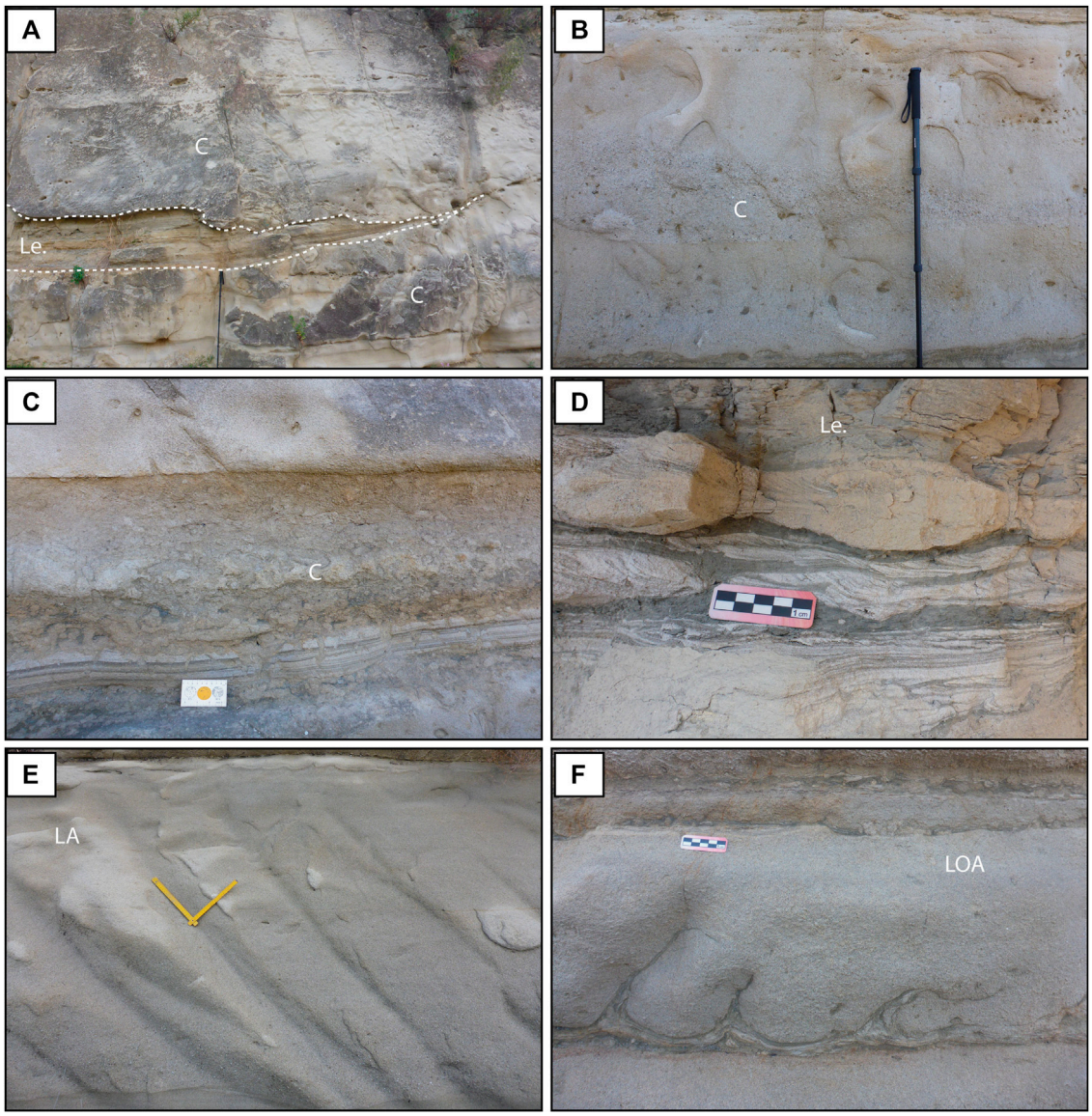

FIGURE 5 | (A) Channel and (C) Levee (Le) facies associations. 1.5 m-long Jacob staff for scale. Levee facies association is locally preserved along channel margins. **(B)** Channel, (C) facies association represented by very coarse-grained sandstones, with pebbly gravel and mud-clasts aligned along large-scale sigmoidal cross-stratification. 1.5 m-long Jacob staff for scale. **(C)** Highly bioturbated siltstones to very fine-grained sandstones commonly preserved at the top of the Channel-Levee (C-Le) facies association. **(D)** Siltstones to very fine-grained sandstones with climbing- and current-ripple structures illustrating the Levee (Le) facies association. **(E)** Lobe axis (LA) facies association represented by weak normal grading, m-thick beds of gravelly to very coarse- and medium-grained sandstones showing parallel lamination. Folding rule meter for scale, 20-cm long segments. **(F)** Lobe off-axis (LOA) facies association illustrated by normally graded coarse- to fine-grained sandstone beds with erosive base and flame structures, alternating with finer-grained deposits with current ripples.

shows multi-reactivation surfaces and lateral migration. Siltstones to very-fine-grained sandstones with climbing- and current-ripple structures are locally preserved below the basal erosive surface (**Figure 5A**). These finer-grained deposits are organized in dm to m-thick packages of 5–10 s m of lateral extent. Horizontal and vertical burrows are common in these fine-grained deposits and paleocurrents, deduced from ripples, and show an oblique flow direction away from the main channel axis. Facies association 1 has a sandstone percentage of 90% based on the reference log section (**Figure 7A**).

Interpretation

These coarse-grained deposits are mostly the product of high-density flows and are similar to the F4–F5 facies tracts described by Mutti (1992) or to the R2-3 and S1-3 divisions of Lowe (1982). Monogenic mud-clast breccias are interpreted as channel-wall collapses or internal levees reworking. Coarse-grained cross-bedded sandstones are interpreted as tractive megadunes. Such cross-bedded layers are similar to the F6 facies of Mutti (1992), Mutti and Normark (1987) and to Lowe's (1982) S1 division, interpreted as the result of waning unidirectional tractive flows

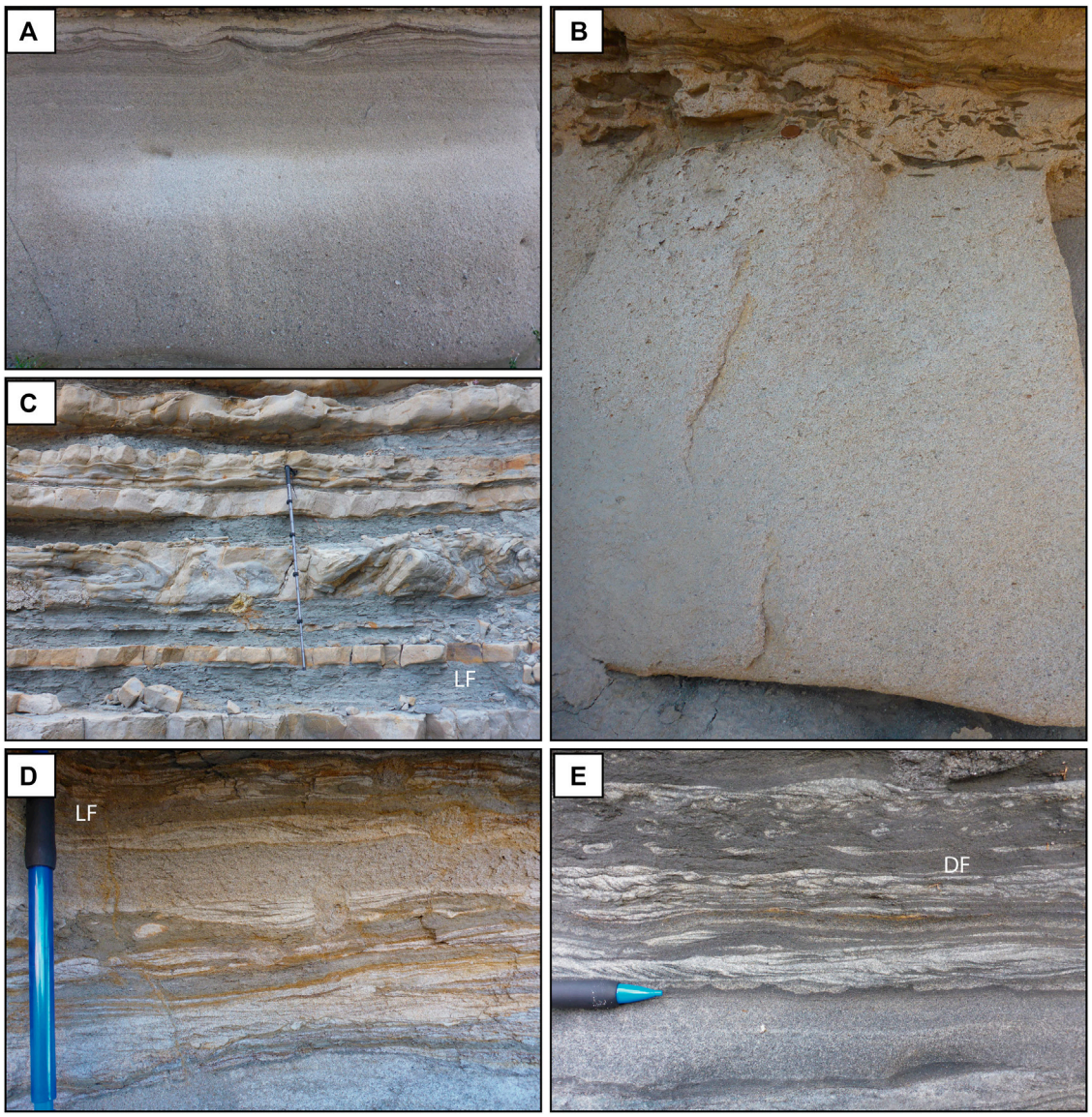

FIGURE 6 | (A) Normally graded gravelly coarse- to very fine-grained sandstone beds with erosive base (Ta-Td), very common in Lobe off-axis (LOA) facies association. Bed is 1-m thick. **(B)** Bipartite bed with a lower division of weakly normally graded coarse- to fine-grained sandstones with rare planar lamination, and an upper division comprising poorly sorted fine- to very fine-grained sandstones with dispersed cm scale mudstone clasts. Lobe fringe (LF) facies association. Bed is 70 cm-thick. **(C)** Lobe fringe (LF) facies association. Massive to normally graded fine- to medium-grained sandstones alternating with shaly-siltstones and siltstones with current ripples. Slump bed is preserved in the thicker bed, in the central part of the photo. 1.5 m-long Jacob staff for scale. **(D)** Shaly-siltstones and siltstones with current ripples of Lobe fringe (LF) facies association. Pencil for scale. **(E)** Distal fringe (DF) facies association. Silty shale intervals containing siltstones and fine- tomediumgrained sandstone beds with plane bed lamination and current ripples. Pencil for scale.

(Mutti, 1992). Fine-grained deposits are interpreted as internal levees preserved in the channel conduit (e.g. Kane and Hodgson, 2011). This facies association is representative for channel-levee turbidite deposits (**Figure 7A**).

Facies Association 2: Lobe Axis (LA)

Description

This facies association is dominated by weak normal grading, 0.1–2 m-thick beds of gravelly to very coarse and medium-grained sandstones showing parallel lamination (**Figure 5E**) with isolated cm-sized mudstone chips aligned parallel to the internal stratification. Overall, beds are moderately to well sorted, and locally contain layers with pebbly gravel commonly preserved at the base of massive beds. Intraformational monogenic mudclasts are observed at bed bases. Bed bases are sharp, loaded, or erosive and can preserve tool marks. Bed amalgamation is common and can lead to 5–10 m-thick packages of massive sandstones. Thick-bedded sandstones show tabular to gently convex-up geometries. They are laterally extensive for up to 50–400 m. Facies association 2 has a sandstone percentage of 94% based on the reference log section (**Figure 7B**).

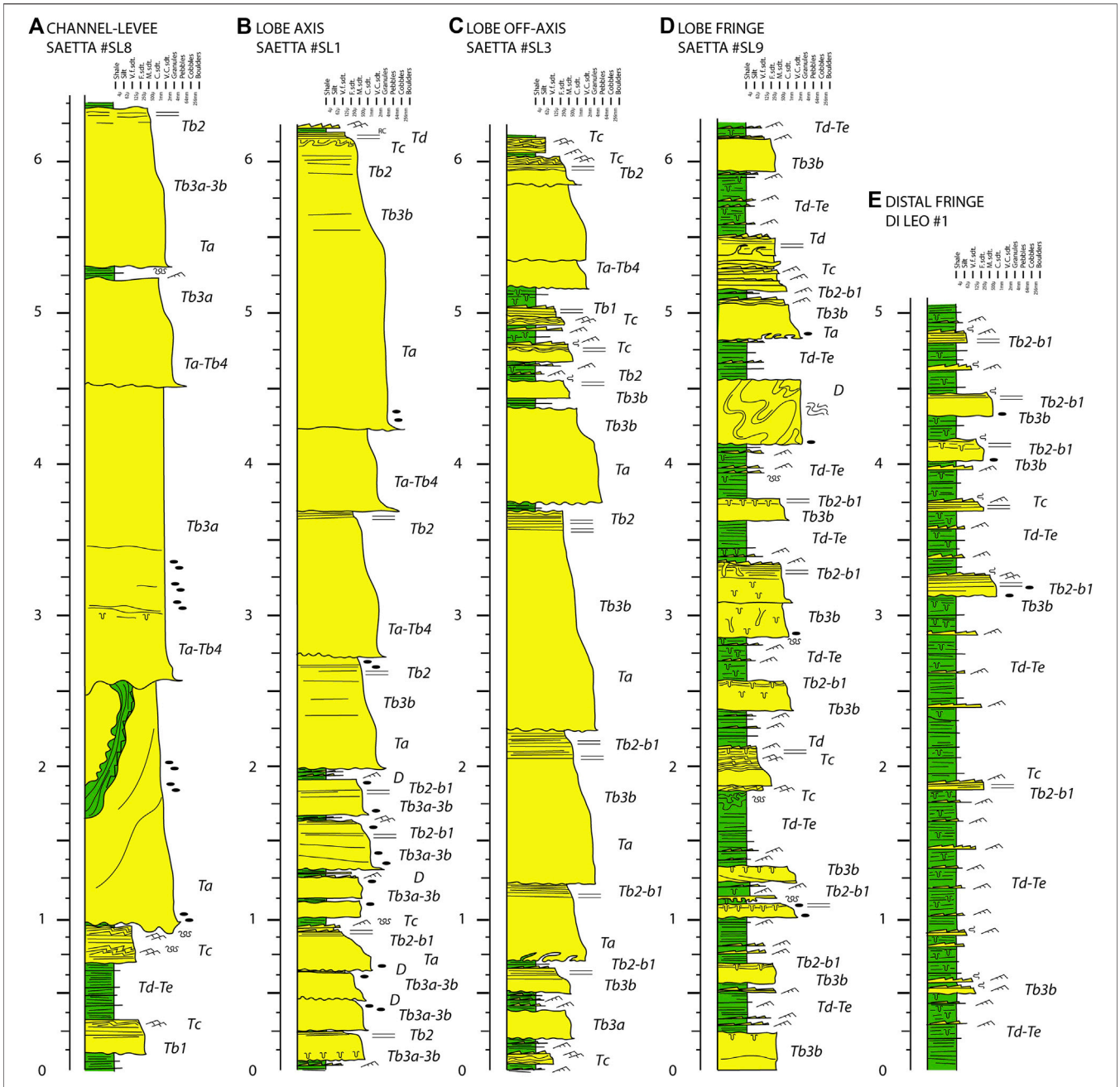

FIGURE 7 | Facies associations and architectural element. **(A)** Channel and Levee (C-Le) from sedimentological section Saetta #SL8. **(B)** Lobe axis (LA) from sedimentological section Saetta #SL1. **(C)** Lobe off-axis (LOA) from sedimentological section Saetta #SL3. **(D)** Lobe fringe (LF) from sedimentological section Saetta #SL9. **(E)** Distal lobe fringe (DF) from sedimentological section Di Leo #1.

Interpretation

Thick-bedded and amalgamated sandstones with weak normal grading are interpreted to be the result of high-density turbidity currents (Kneller and Branney, 1995) with high aggradation rates (Arnott and Hand, 1989; Leclair and Arnott, 2005; Talling et al., 2012). Coarse- to medium-grained sandstones, well-sorted, with well-developed plane-parallel lamination are equivalent to the F7–F8 facies tracts of Mutti (1992). The geometries, thickness, and facies conform to lobe- or channel-axis settings (**Figure 7B**; e.g., Prélat et al., 2009; Brunt et al., 2013; Spychala et al., 2015).

Facies Association 3: Lobe Off-axis (LOA)

Description

This facies association comprises very coarse- to very-fine-grained, normally graded sandstone beds that are well sorted (**Figures 5F**, **6A**). Bed thicknesses range from 0.1 to 1 m.

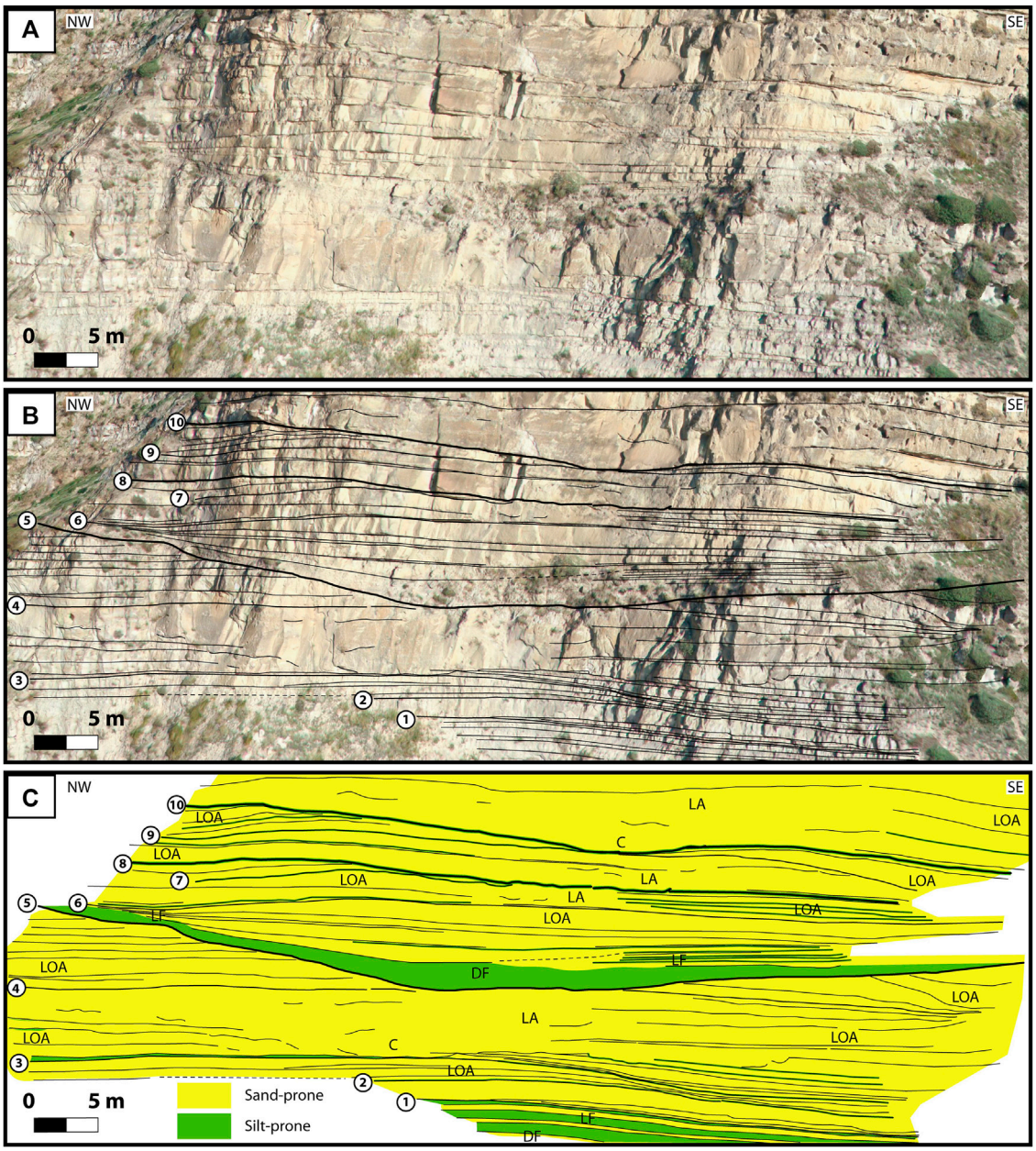

FIGURE 8 | Stratigraphic architecture of the Motta area illustrating Channel-Lobe transition zone. Panoramic view extracted from the 3D outcrop model **(A)** and interpretation **(B,C)**. The main surfaces discussed in the text (1–10) are highlighted. Surfaces at the top of lobe are represented by thicker dark lines (Lines 5, 8, and 10). Lobes are composed of several lobe elements. (C) Channel, (Le) Levee, (LA) Lobe axis, (LOA) Lobe off-axis, (LF) Lobe fringe, (DF) Distal lobe fringe. See *text* for further explanations.

Observed sedimentary structures include planar lamination (Tb), wavy lamination, current-ripple lamination, and climbing ripple lamination (Tc), locally organized in a repetitive pattern. Bed bases are sharp or loaded with flame structures (**Figure 5F**). Bed tops are sharp and commonly eroded (**Figure 5F**). Medium- to thin-bedded sandstones show tabular to convex-up geometries and can be traced for 10's to 100's of meters down-dip and in the strike section. Facies association 3 has a sandstone percentage of 85% based on the reference log section (**Figure 7C**).

Interpretation

Bedforms such as planar lamination and current-ripple lamination are produced beneath dilute turbulent flows, which rework sediment along the bed (Allen, 1982; Southard, 1991; Best and Bridge, 1992). Thin beds with repeating patterns of climbing-ripples and planar lamination are interpreted to indicate highly unsteady flow behavior (Jobe et al., 2012). This facies association is interpreted to be deposited by high- to low-density turbidity currents in a lobe off-axis setting (**Figure 7C**; e.g. Spychala et al., 2015).

Facies Association 4: Lobe Fringe (LF)

Description

Beds are predominantly composed of fine- to medium-grained sandstones alternating with shaly-siltstones and siltstones (**Figure 6C**). Sandstone beds range in thickness from a few cm up to several dm and form flat to convex-up lens-shaped bodies pinching out over tens of meters. Sandstone beds show planar, current-ripple, or wavy laminations, whereas siltstone beds commonly display planar lamination with isolated starved ripples (**Figure 6D**). Shaly-siltstones and siltstones are commonly burrowed. Some beds show bipartite structure with a lower division of weakly normally graded fine-grained sandstones with rare planar lamination and thin mudstone-clast layers, and an upper division comprising poorly sorted very fine-grained sandstones and siltstones with dispersed mm-cm scale mudstone clasts (**Figure 6B**). The contact between the two divisions is commonly sharp and undulating. Slumps and contorted beds are common, ranging in thickness from a few dm up to several dm (**Figure 6C**). Slump beds are commonly truncated at top. Facies association 4 has a sandstone percentage of 45% based on the reference log section (**Figure 7D**).

Interpretation

Ripple lamination formed due to reworking by dilute turbulent flows with moderate aggradation rates, whereas climbing-ripple lamination is indicative of high aggradation rates (Allen, 1971, 1982; Southard, 1991). Bipartite beds are interpreted as hybrid event beds (Haughton et al., 2009) which primarily occurred at the bases and fringes of lobe deposits (e.g., Hodgson, 2009; Talling, 2013). Spychala et al. (2017) confirmed the lobe fringe setting for bipartite beds using a statistical approach on the Karoo example, but suggested that the occurrence at the bases was rather an artifact of lobe stacking. Ripple and planar laminated packages correspond to the Tb, Tc, and Td divisions of the Bouma sequence (1962) respectively, and shaly siltstones to Te. The abundance of Tb2, Tb1 layers in cm-thick beds indicates deposition from low-density subcritical flows (cf. Arnott and Al-Mufti, 2017; Postma and Kleverlaan, 2018). The heterolithic alternations could result from varying discharge to produce a stack of alternating low- and high-density turbidite deposits (Postma and Kleverlaan, 2018). The tabular geometry of beds in the lens-shaped convex-up bodies indicates unconfined sheet flow from an outlet point source. The intercalated and burrowed shaly siltstones suggest that outlet stability lasted for a period of time and was not related to just one flow event. Observed facies and thicknesses of this facies association conform to an interpretation of a lobe-fringe setting (**Figure 7D**).

Facies Association 5: Distal Fringe (DF)

Description

Thick bioturbated claystone to silty shale intervals contain rare siltstones and fine- to medium-grained sandstone beds with plane bed lamination and ripple crossbedding (**Figure 6E**). Rare well-sorted sandstone beds are tabular with a few cm in thickness displaying Tb2-Tb1-Tc. Some beds incorporate mudstone chips. The claystone to silty shale intervals are too strongly bioturbated and poorly outcropping to be studied in further detail. Facies association 5 has a sandstone percentage of 15% based on the reference log section (**Figure 7E**).

Interpretation

Structureless beds are attributed to direct suspension fallout (Te of Bouma, 1962), whereas planar laminated beds are commonly interpreted as the product of traction processes (Stow and Piper, 1984; Mutti, 1992; Talling et al., 2012). Siltstone and thin sandstone beds (Tb2-Tb1-Tc) are interpreted as the preserved products of low-density turbidity currents. The low-density turbidity currents are characterized by bedload transport producing plane bed Tb1 term and Tc current ripples term (Postma and Cartigny, 2014). The geometries, thickness, and facies conform to a low-energy depositional environment in distal lobe-fringe settings (**Figure 7E**).

Facies Association 6: Hemipelagic Background

Description

Homogenous intervals of silty shale to claystone are mainly preserved at the base of the Motta San Giovanni Formation (Motta 1 of Barrier, 1987). Layers of concretions are common and tend to be associated with distinct horizons associated to fauna, including cephalopods, scaphopods, pelecypods, gastropods, bryozoans, brachiopods, fish remans, echinoderms, and deep-water corals. Claystone intervals are laterally extensive for kilometers. Very thin-bedded (mm-scale) graded siltstone layers showing occasionally current-ripple cross stratification, are locally intercalated with claystone. Facies association 6 has a sandstone percentage of less than 2%.

Interpretation

Claystone are interpreted as hemipelagic background deposits. Where mapped over large areas, they mark episodes of sediment starvation in the deep basin and are interpreted to contain the deep-water expression of maximum flooding surfaces (e.g., Flint et al., 2011). Starved current-ripples in fine-grained deposits could be interpreted as resulting from the action of bottom currents or phases of major turbiditic inputs.

DEPOSITIONAL MODEL AND ARCHITECTURE

Motta area: Channel-lobe Transition Zone (*CLTZ*)

Description

The Motta area was studied in more detail in a 70 m long and 25 m high section extracted from the 3D outcrop model, which is part of a large outcrop (1.2 km long, 400 m high, **Figure 8**). Ten main surfaces were identified and describe the overall architecture and stacking pattern. The architecture shows a prograding trend from distal lobe fringe and hemipelagic background facies associations to lobe axis and channel facies associations.

A coarsening and thickening upward trend is observed from below surface 1 up to surface 2. The geometry of beds is

organized in lens-shaped convex-up bodies (Surface 2, 1 m-high convex-up feature) showing lateral compensation of isolated, or detached lobes. The same pattern characterizes the beds up to surface 3. This lower part of the outcrop shows a succession of prograding cycles from distal lobe-fringe to lobe off-axis facies associations. The lateral and abrupt facies change from the lobe axis to the lobe off-axis, on both the sides, is illustrated between surfaces 3 and 4. Locally, the channel facies association is observed. This unit is also organized in an overall prograding to aggrading trend. A preferential lateral migration of the lobe axis facies association is observed toward the southwest. From surfaces 4–5, the unit is characterized by an abrupt lateral migration and progradation of lobe off-axis facies association, on both sides, associated with the enlargement of an erosive and bypass surface (surface 5, 3–5 m deep). Surface 5 is draped by very fine-grained deposits from distal fringe to hemiplegic background facies associations.

The following unit from surfaces 5–6 is organized in lens-shaped convex-up bodies (3–4 m-high) showing a prograding and aggrading trend from distal lobe-fringe to lobe off-axis facies associations. Surface 5 paleo-relief is progressively filled to finally generate convex-up bodies. The lateral and abrupt facies change from the lobe axis to the distal lobe fringe is observed on both the sides in less than 40 m. From surfaces 6–7, the unit shows the same pattern as unit delimited by surfaces 3 and 4. Lateral and abrupt facies change from the lobe axis to the distal lobe fringe is also observed on both the sides, with a preferential lateral migration to the southwest. From surfaces 7–8, the unit is organized in an abrupt lateral migration associated with the progradation of the overlying erosive and bypass surface (surface 8, 1-m deep).

From surfaces 8–9, the unit shows the lateral facies change from the lobe axis to the lobe off-axis, on both the sides, forming lens-shaped convex-up bodies (2–3 m-high). Unit is organized in an aggrading trend. The following unit (surfaces 9–10) is characterized by an abrupt lateral migration and progradation of the lobe off-axis facies association, on both the sides, associated with the enlargement of an erosive and bypass surface (surface 10, 2–4 m deep). Above surface 10, a 5 to 8 m-thick massive unit is organized in an aggrading, gently prograding trend.

Interpretation

Field data show a consistent stratigraphic hierarchy, which favors an intrinsic morphodynamic process rather than a random one for lobe development. The documented facies associations reoccur in each unit and show a consistent trend at the scale of the unit (2–10 m-thick) and even higher. The identified individual units are interpreted as lobe elements (for example between surfaces 3 and 4) organized at larger scale in lobes (for example between surfaces 1 and 5). The first documented lobe, between surfaces 1 and 5, illustrated the complete cycle from distal lobe fringe and hemiplegic background facies associations to final erosive and bypass surface (surface 5). Each lobe element corresponds to a major stage of the lobe evolution, with *1*) detached and isolated lobes, *2*) prograding-aggrading lobe, *3*) abrupt lateral migration associated with lobe overflow, spillovers, and major bypass, and *4*) finally abandonment. The second lobe (surfaces 5–8) is organized in a similar pattern. The two overlying lobes only show the two final stages with a more proximal character, suggesting that the detached and isolated lobes of the first stage are preserved down-dip.

The area is dominated by the lobe axis facies association and major bypass and erosive surfaces. These features are interpreted as representative of the channel-lobe transition zone (CLTZ) to very proximal part in the lobe (e.g. Wynn et al., 2002; Pyles et al., 2014; Hofstra et al., 2015; Hodgson et al., 2016; Brooks et al., 2018).

Saetta Area: Stacked Lobes

Description

The Saetta panorama is 90 m long for 35 m high (**Figures 9**, **10**). Thirteen main surfaces were highlighted to describe the overall architecture and stacking pattern.

A coarsening and thickening upward trend is observed from below surface 1 up to surface 2 (**Figures 7B**, **10**). The geometry of beds is organized in lens-shaped convex-up bodies (Surface 2) showing lateral compensation. These beds are organized in a prograding cycle from hemipelagic setting, to distal lobe-fringe then lobe fringe facies associations. From surfaces 2 to 3, the unit is organized in a rapid progradation from distal lobe-fringe to lobe fringe facies associations, and then a thick aggrading trend from lobe-axis to channel facies associations. Surface 3 is erosive, and draped with mud clast lags, as well as well-preserved reddish crust. The same pattern is observed between surfaces 3 and 4. This unit also shows the abrupt lateral facies change from the lobe axis to the lobe off-axis and lobe fringe in less than 90 m. Surface 4 is highly erosive (2-m deep) and the highest erosion is localized just on the top of the former lobe axis. The same prograding-aggrading pattern is observed between surfaces 4 and 5 and the facies belts compensate and fill the previous relief. Surface 5 is highly erosive and could entirely crosscut the previous unit down to surface 4. Surface 5 is draped by fine-grained deposits with climbing ripples diagnostics for the internal levees facies association. From surfaces 5 to 6, the paleo relief is progressively filled by m-scale prograding cycles made of lobe fringe to lobe axis facies association organized in an overall back stepping trend. Between surfaces 6 and 7, a last m-scale prograding cycle finally seals the former paleo relief by a progressive lobe compensation. All these small-scale cycles show the lateral facies change from the lobe axis to the distal lobe fringe in less than 90 m. Surface 7 is convex-up and draped with a reddish crust.

From surfaces 7 to 10, three units are organized in an overall prograding trend, and are themselves internally organized in a similar manner. These cycles illustrated the complete lateral facies change from the distal lobe fringe to the lobe axis and channel facies associations in less than 100 m.

Surface 10 is erosive (1–2 m-deep). It is associated with channel-levee facies association that rapidly laterally passes to lobe off-axis and lobe fringe facies association (<100 m).

From surfaces 11 to 13, m-scale prograding cycles are organized in an overall backstepping trend. Surface 13 is convex-up and draped with a reddish crust.

Interpretation

Intrinsic morphodynamical process rather than a random process for lobe development is one more time favored based on these

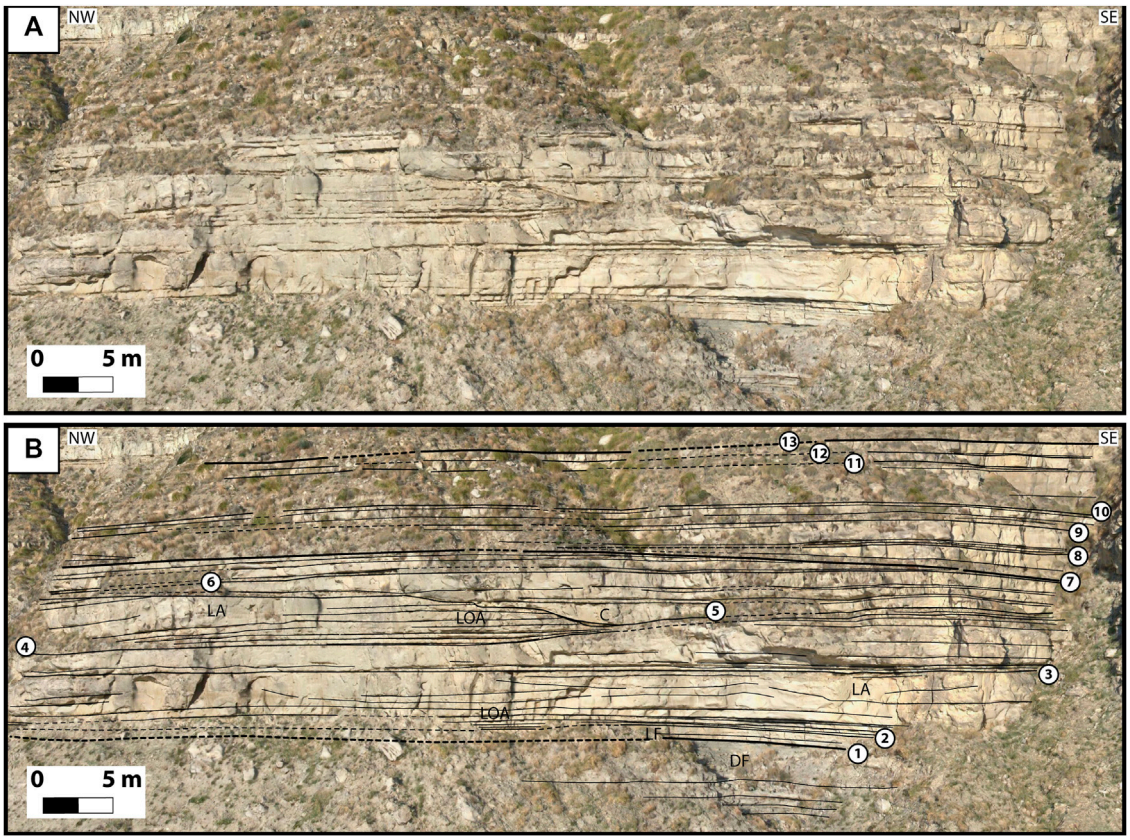

FIGURE 9 | Stratigraphic architecture of the Saetta area illustrating stacked lobes. **(A)** Panoramic view extracted from the 3D outcrop model. **(B)** The main surfaces discussed in the text (1–13) are highlighted. Surfaces at the top of lobe are represented by thicker dark lines (e.g. Lines 7 and 13). Full interpretation is presented in **Figure 10**. (C) Channel, (Le) Levee, (LA) Lobe axis, (LOA) Lobe off-axis, (LF) Lobe fringe, (DF) Distal lobe fringe.

observations. The individual identified units are interpreted as lobe elements (for example between surfaces 3 and 4) organized into lobes at a larger scale (for example between surfaces 1 and 7). Two main lobes are illustrated with the Saetta panorama. From surfaces 1 to 7, the lobe is organized with *1*) a prograding trend from hemipelagic setting, to distal lobe-fringe then lobe axis facies associations (up to surface 3), then *2*) an aggrading trend with lateral lobe compensation (up to surface 5), *3*) a deep erosion and bypass, followed upward by *4*) a backstepping trend. At the lobe element scale, the first three stages are well recorded; nevertheless, the backstepping trend is coeval with a starved and bypass surface (for example surface 3). The second lobe shows more distal facies associations, but with a similar organization characterized by *1*) prograding and *2*) aggrading trends (from surfaces 7 to 10), *3*) deep erosion and bypass on surface 10, and *4*) filling of the paleo relief and backstepping trend.

Di Leo Area: Isolated or Detached Lobe

Description

The selected Di Leo panorama is 350 m-long and 6 m high (**Figures 11**, **12**). Three main surfaces were highlighted to describe the overall architecture and stacking pattern of this outcrop (**Figure 11**).

Below surface 1, highly bioturbated fine-grained siltstones to medium-grained sandstones do not preserve primary sedimentary features. They share similarity with hemipelagic setting to distal lobe-fringe facies associations. Surface 1 corresponds to a sharp surface, locally erosive (>0.5 m deep) with tool marks and loading features in proximal area. Surface 1 is progressively conformable in the most distal part (**Figure 11**). The geometry of the beds is organized in lens-shaped convex-up bodies, up to surfaces 2 and 3. Surface 2 is a convex-up intermediate surface (**Figure 11**). Lobe off-axis to lobe axis faces association are dominant between surfaces 1 and 2. From surfaces 1 to 3, the unit covers the complete depositional profile from channel to lobe axis, and distal lobe fringe facies associations, in less than 350 m. Large-scale oblique backsets are observed in the lobe axis to channel facies associations (**Figure 12**). Bioturbations are well preserved on the lobe crest. Surface 3 corresponds to a sharp surface with a reddish crust, current- and undulating ripples. Hemipelagic setting to distal lobe-fringe facies associations onlap onto surface 3.

Interpretation

In the Di Leo area, beds, lobe elements, and lobe are of the same order, i.e. 1–3 m thick. The observed lobe is 350 m-long and has a maximum thickness of 3 m. The lobe is not directly connected to any channel-levee system and is fully interbedded within distal

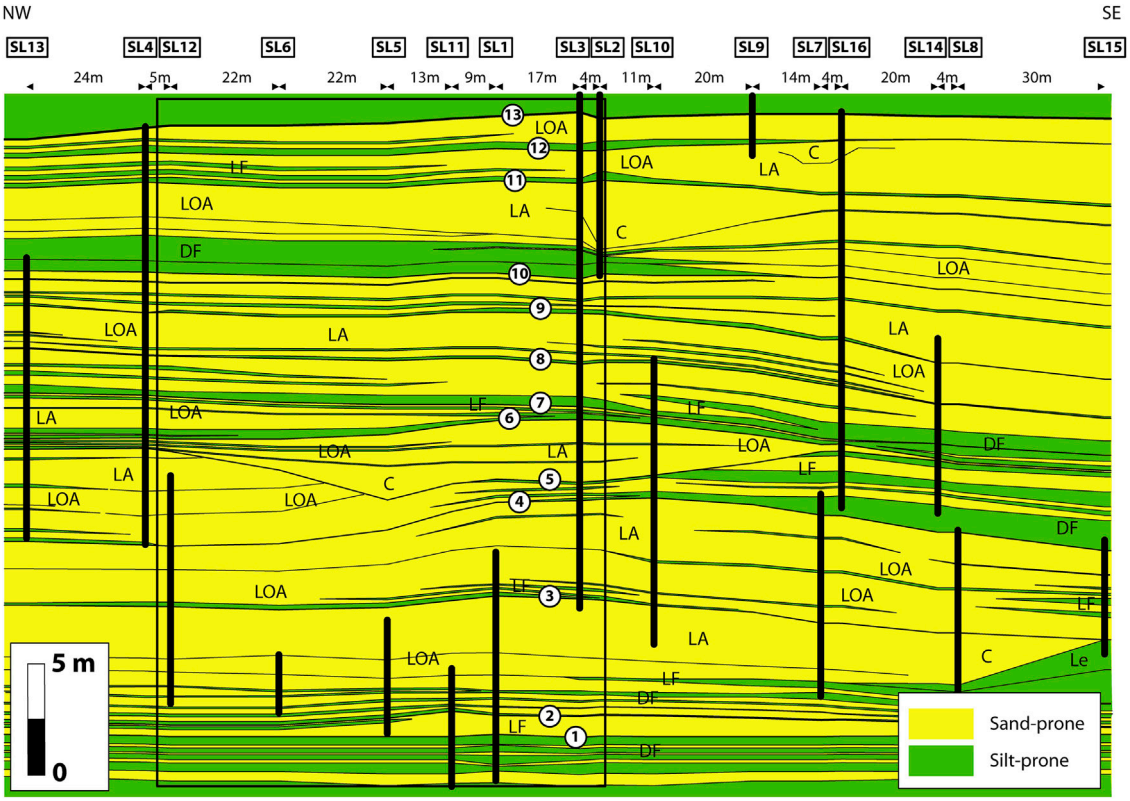

FIGURE 10 | Correlation panel of the Saetta area illustrating stacked lobes. The black rectangle corresponds to **Figure 9** with horizontal extension from sedimentological section SL12 to SL2. Thick vertical black lines correspond to the sedimentological sections. (C) Channel, (Le) Levee, (LA) Lobe axis, (LOA) Lobe off-axis, (LF) Lobe fringe, (DF) Distal lobe fringe.

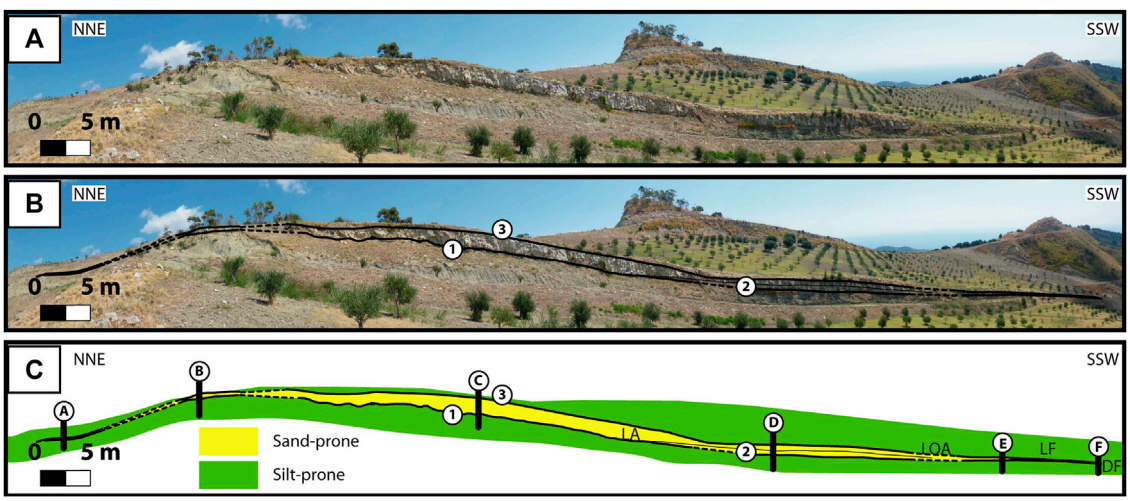

FIGURE 11 | Panoramic view of the Di Leo area illustrating the isolated detached lobe architecture. The main surface discussed in the text (1–3) is highlighted. Sedimentological sections **(A–F)** and interpretation are presented in **Figure 12**. Channel (C) facies association is preserved up dip of the Lobe axis (LA) facies association. (C) Channel, (LA) Lobe axis, (LOA) Lobe off-axis, (LF) Lobe fringe, (DF) Distal lobe fringe.

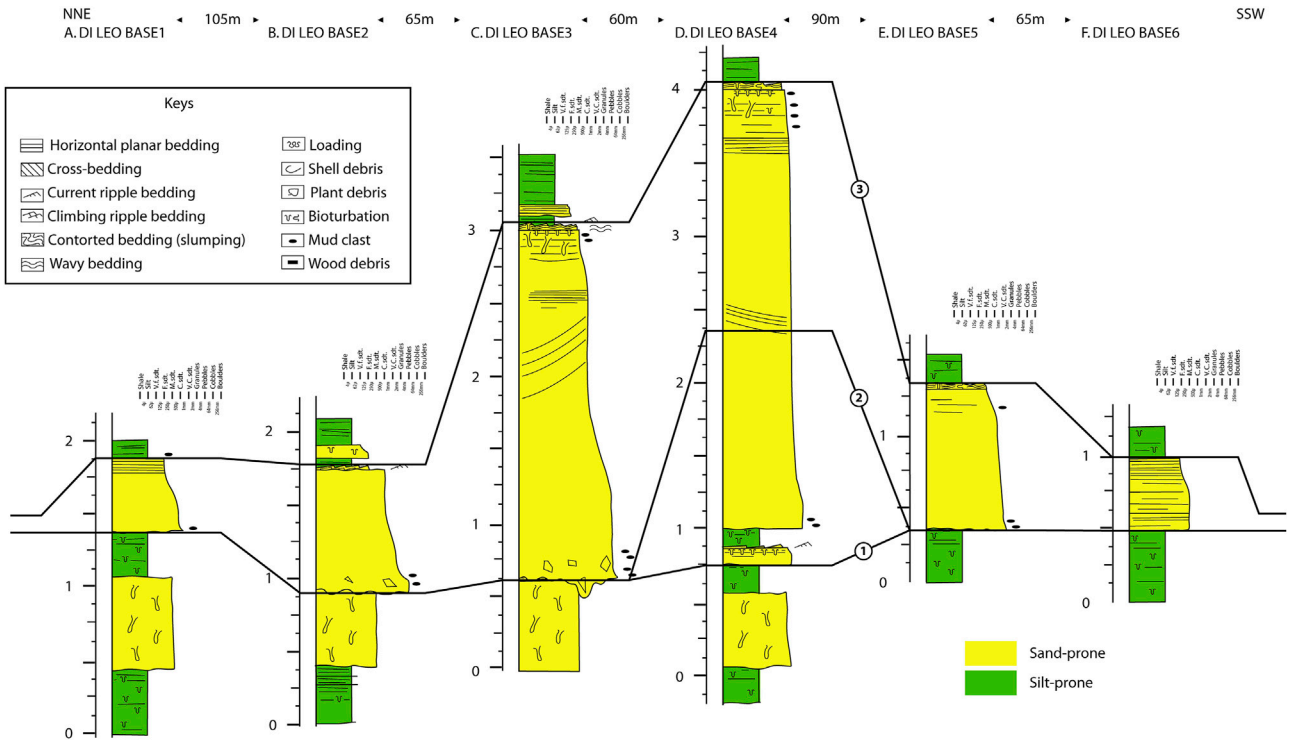

FIGURE 12 | Correlation panel of the Di Leo area illustrating an isolated detached lobe. Surface 1 is erosive in the proximal area (NNE) and progressively conformable in the most distal area (SSW). Rapid progradation is illustrated between surfaces 1 and 2. Prograding to aggrading trend is illustrated between surfaces 2 and 3.

facies association (**Figures 11**, **12**). We interpret the lobe evolution in three main stages with: *1*) channel, lobe conduit, and lobe initiation (from surfaces 1 to 2), *2*) channel extension, lobe progradation, and aggradation (from surfaces 2 to 3), and *3*) lobe abandonment and bypass potentially related to avulsion (surface 3). These main stages are very similar to those of the small-radius sand-rich fan lobes of Postma and Kleverlaan (2018).

DISCUSSION

Characteristics of Perched Lobe Deposits in the Motta San Giovanni Formation

Dimensions

The studied lobes are characterized by an overall convex-up morphology, locally flat or even gently concave-up in their middle axial part and with steeper slopes on their sides. The lobe dimensions were calculated using the 3D outcrop models for the three studied areas (**Table 1**). These lobes are architectural elements with a width of 300–3000 m, a length of 500–5000 m, and thicknesses between few to tens of meters (2–22 m thick). A stack of several lobes forms a lobe complex with a thickness of several 100's of meters (*sensu* Prélat et al., 2009; Etienne et al., 2012; Spychala et al., 2017). Lobes are composed of stacked lobe elements that are two to ten times smaller in width and thickness.

The width/max-thickness ratio is low when comparing with confined, and even more with unconfined turbidite system (**Figure 13**). Confined systems have generally lower width/max-thickness ratio when compared to unconfined system. The two domains are distinct with a relative superimposition. The overall trends from bed, to lobe element, lobe, and lobe complex are very similar (power law relationship) in the two domains, as well as the limit between the two domains. For example, in the Annot system, which is a text-book example for confined system, lobe width is ca. 1–5 km, for a thickness of 2–10 m (Moraes et al., 2004). Lobe width is commonly two to three times higher and thickness up to two times smaller than the studied lobes. The intraslope lobes of the Karoo basin (Spychala et al., 2015) are three to ten times larger, with the same thickness ranges, than the Motta San Giovanni lobes. In the Zaire system, which is a representative unconfined example, lobe width is ca. 10–40 km, for a thickness of 5–10 m (Jegou et al., 2008), that is ten to hundreds of times larger in width, with the same order of magnitude in thickness than the studied examples.

There is considerable variation both laterally and vertically, resulting in a complex distribution of architectural elements in the Motta San Giovanni lobes. As the lobe sizes are two to five times smaller than the tilted fault block width (**Figure 4**), and the paleocurrents show a clear relationship with normal fault orientation, we suggest that active tectonics influenced the intraslope lobe deposition, both in terms of topographic variation and subsequent lateral stacking. On the Log-log plots

TABLE 1 | Dimensions of Lobe Complexes, Lobes and Lobe elements in the Motta San Giovanni Formation (Miocene, Calabria) quantified from the 3D outcrop models.

Formation	Age	Type	Mode	Lobe width (m)	Lobe maximum thickness (m)
Motta San Giovanni	Miocene	Lobe Complex	Confined	4000	200
Motta San Giovanni	Miocene	Lobe Complex	Confined	5000	400
Motta San Giovanni	Miocene	Lobe Complex	Confined	4000	150
Motta San Giovanni	Miocene	Lobe Complex	Confined	6000	500
Motta San Giovanni	Miocene	Lobe	Confined	500	14
Motta San Giovanni	Miocene	Lobe	Confined	1000	17
Motta San Giovanni	Miocene	Lobe	Confined	1500	20
Motta San Giovanni	Miocene	Lobe	Confined	1000	22
Motta San Giovanni	Miocene	Lobe	Confined	300	10
Motta San Giovanni	Miocene	Lobe	Confined	290	3
Motta San Giovanni	Miocene	Lobe	Confined	600	9
Motta San Giovanni	Miocene	Lobe	Confined	800	15
Motta San Giovanni	Miocene	Lobe	Confined	600	15
Motta San Giovanni	Miocene	Lobe Element	Confined	400	4
Motta San Giovanni	Miocene	Lobe Element	Confined	200	7
Motta San Giovanni	Miocene	Lobe Element	Confined	110	4
Motta San Giovanni	Miocene	Lobe Element	Confined	105	4
Motta San Giovanni	Miocene	Lobe Element	Confined	200	5
Motta San Giovanni	Miocene	Lobe Element	Confined	500	4

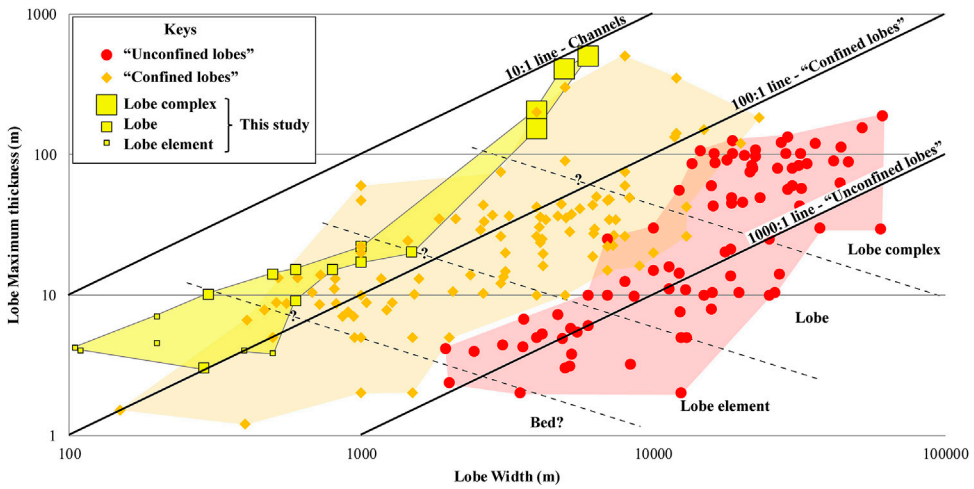

FIGURE 13 | Observed width vs. maximum thickness for studied lobes of the Motta San Giovanni Formation (green square), plotted on the log-log plot with confined systems aligned on a 100:1 line (diamond in different shades of yellowish) and unconfined systems aligned on a 1000:1 line (dot in different shades of bluish). 10:1 line illustrates the trend for channels (Pickering and Clark, 1996). Data are extracted from Pirmez et al. (2000), Bruhn et al. (2003), Moraes et al. (2004), Prélat et al. (2009, 2010, and reference therein), Etienne et al. (2012), Spychala et al. (2015), Marini et al. (2016), Picot et al. (2016, and reference therein), and Postma and Kleverlaan (2018), McArthur et al. (2021).

of widths vs. maximum thicknesses, our population is intermediate between 10:1 trend of channels (Pickering and Clark, 1996) and 100:1 line of confined systems (**Figure 13**). The transform margin perched lobes of the Motta San Giovanni Formation can be considered end-members taking into account the width/max-thickness ratio criteria.

Net-to-Gross, Facies, and Processes

In the Motta San Giovanni lobes, facies transitions occur over very short distances, typically over 10's of meters. It is consistent with other intraslope lobe systems, such as the Karoo one (Spychala et al., 2015). It is a striking difference when comparing with basin floor lobe systems characterized by facies transitions over several kilometers (e.g., Prélat et al., 2009; Groenenberg et al., 2010).

The Motta San Giovanni lobes are characterized by a very high percentage of sandstone (>90–95% in lobe axis), probably because the upper fine-grained part of the flow can be stripped downdip, overpassing the confined lows along the slope, which will increase the relative proportion of sand that

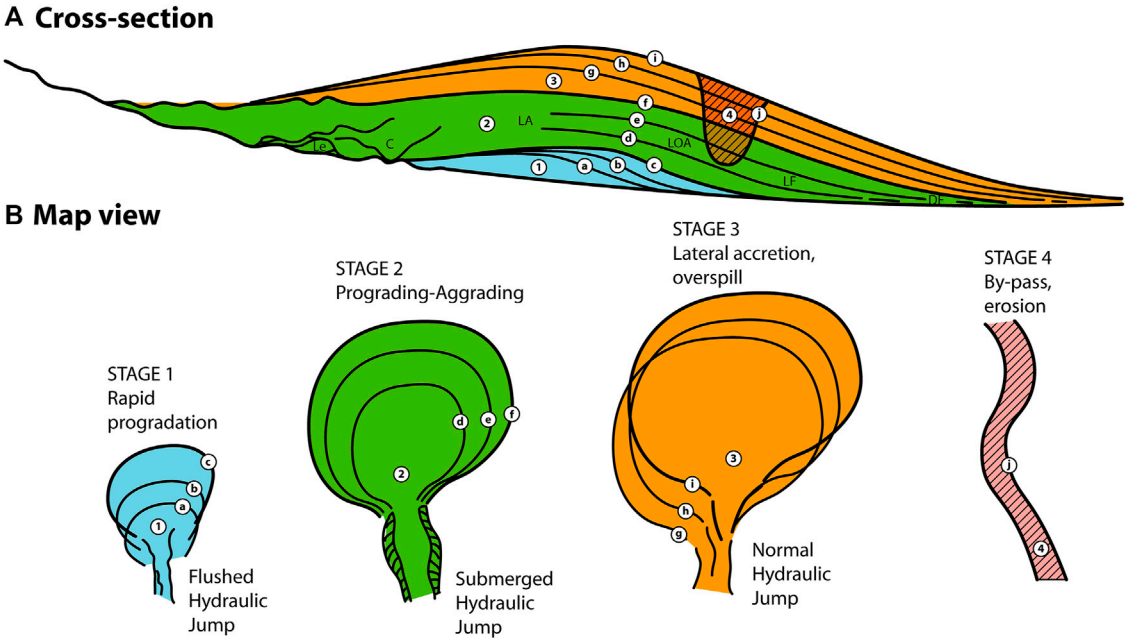

FIGURE 14 | Depositional model for intraslope lobes based on the Motta San Giovanni Formation (Miocene, Calabria). Stage 1: increasing sediment supply associated with rapid progradation of the lobe in response to flushed hydraulic jump in the Channel-Lobe transition zone. Stage 2: high sediment supply in balance with depositional processes and accommodation space resulting in a prograding-aggrading trend. Channel-Levee (L-Le) facies association is well preserved directly up dip to the Lobe axis (LA) facies association. Stage 3: high sediment supply is not at equilibrium with accommodation space and depositional system size resulting in overspill processes and lateral accretion. Stage 4: unstable and unbalance system recorded by bypass and erosion progresses.

is locally accumulated. Such bypass and overspill processes are typical of intraslope sub-basins as also described from other geological contexts (Sinclair and Tomasso, 2002; Prather, 2003; McArthur et al., 2021).

Studied lobe fringes record few bipartite beds, which are diagnostic for basin floor lobe fringe deposits (Hodgson, 2009). It is in line with the observation from the intraslope lobe fringe deposits of the Karoo example (Spychala et al., 2015).

Stacking Pattern and Incisions

The studied lobes show cyclicity recorded at the lobe element scale with prograding to prograding-aggrading trends that are very common in many lobes (e.g., Guillocheau et al., 2004; Gervais et al., 2006; Deptuck et al., 2008; Prélat et al., 2009; Mulder and Etienne, 2010; Postma and Kleverlaan, 2018). An aggradational to slightly compensational style of stacking is also observed in the Motta San Giovanni lobes (Motta and Saetta areas) that are present in other intraslope and confined lobes (Guillocheau et al., 2004; Spychala et al., 2015). In contrast, basin floor lobes exhibit markedly compensational styles of stacking to form wide and spread lobe systems (Prélat et al., 2009; Groenenberg et al., 2010; Straub and Pyles, 2012).

Another diagnostic staking pattern feature has been observed with m-deep erosion and bypass surface at the top of the lobe, and locally of lobe elements (Motta and Saetta areas). These surfaces and related paleo relief are rarely filled with channel-like facies association suggesting the system to be very instable. Intraslope lobes are commonly incised by channels in response to transient slope accommodation (e.g., Adeogba et al., 2005; Spychala et al., 2015).

Lobe Depositional Model in Intraslope Complex Margin

Based on the Motta San Giovanni examples, we propose a depositional model including four stages of evolution for intraslope lobes deposited in perched mini-basins organized in piano-like blocks along transform margins (**Figure 14**).

Stage 1 corresponds to channel and lobe initiation on fine-grained deposits (substrate) with elongate fan-lobe elements (**Figure 14**). This stage is for example illustrated between surfaces 1 and 2 in Motta and Saetta areas (**Figures 8–10**). Lobe elements show coarsening and thickening upward trends indicating progradational stacking of distal lobe facies associations. There is no deposition in the CLTZ during stage 1, but rather bypass and erosion. The hydraulic jump is flushed all over the CLTZ resulting in isolated, detached lobe. Stage 1 could be considered the lobe precursor. The lobe precursor generally corresponds to a single or a few lobe beds.

Stage 2 records both progradation and aggradation of lobe elements that are coarser grained than those of the distal lobe facies association observed in stage 1 (**Figure 14**). This stage is for example illustrated between surfaces 3 and 4 in the Motta area (**Figure 8**), as well as between surfaces 2 and 3 in the Saetta area (**Figures 9**, **10**). Channel, lobe axis to lobe fringe facies

associations are vertically stacked and progressively onlap on the former CLTZ. This aggradation of the most proximal facies association locally reduces the depositional slope gradient in the CLTZ. We propose that the hydraulic jump was progressively submerged inducing energy loss. We interpret stage 2 as recording a balance between sediment supply and accommodation space within the active lobe area.

Stage 3 is characterized by major bypass associated with lateral accretion, with locally aggradation (**Figure 14**). This stage is, for example, illustrated between surfaces 4 and 5 in the Motta area (**Figure 8**). Lobe shows overflow and spill over geometries suggesting a down-dip migration of the hydraulic jump across the propagating CLTZ on the top on the former lobe at the end of stage 2. Observed facies and geometries do not support a major progradation of the feeder channel-levee complex during this stage, but rather bypass processes in the CLTZ. The width of the lobe axis progressively increases, while other parts of the lobe start to be starved.

Stage 4 is characterized by bypass and starved deposits (reddish crusts) draping the previous paleo-relief on the top of the former lobe at the end of stage 3 (**Figure 14**). Surface 3 in the Di Leo area illustrates Stage 4 (**Figures 11**, **12**). No (to very thin) channel-levees (facies association 1) are preserved in the former and initial upstream CLTZ. Deep incision across lobe or in inter lobe area suggests major final bypass and erosion, potentially in response to cascading effect on previous lobe morphology. Erosion along surface 5 in the Saetta area is a good example of Stage 4 (**Figures 9**, **10**).

This dynamic shares similarities with the model proposed by Postma and Kleverlaan (2018), and their comparison to the experimental study of Hamilton et al. (2015), especially stages 1 and 2. There is nevertheless an important difference because, in their models, after the prograding-aggrading phase (Stage 2), the hydraulic jump subsequently retreated upstream over time, and avulsed to create a new channel. This point initiates the back-fill stage 3 of Postma and Kleverlaan (2018). In contrast, our stage 3 based on the Motta San Giovanni Formation cannot be considered a simple avulsion with a new cycle, as it is repetitive in many lobe-stacking patterns and records a renewal normal hydraulic jump occurrence. We interpret stage 3 as recording a progressive unbalance between available accommodation space and sediment supply. The entire lobe area would thus not be fully covered by deposition and lateral migration, thus over spilling initiated. Our stage 4 is also not comparable with the back-filling stage of Postma and Kleverlaan (2018) as it records both bypass and abrupt lobe abandonment with starved deposits. It suggests that the main period for sediment bypass through the basin floor fan is mainly recorded by a condensed bypass surface localized at the top of the lobe (Stage 4).

The proposed evolution model also shares similarities with the conceptual model of confined sandy margin of the late Quaternary Golo system established by Gervais et al. (2004, 2006). In the Golo system, the quantity and quality of sediment supply to the basin are controlled by the relative sea level changes and potential connection between canyon and sediment source. Our stage 1 could fit with the lowering sea level and intermediate turbidity activity stage characterized by large thin sand lobes deposits. Our stage 2 could fit with the lowstand sea level phase characterized by large, thick, and stacked sand lobes deposits. It is not clear if our stage 3 fits with the previous stage or with the following rising sea level one characterized by moderate turbiditic activity with small thin sand deposits. The interglacial high stand setting could correspond to hemipelagic sedimentation preserved in between lobes. The model proposed by Gervais et al. (2004, 2006) nevertheless lacks our stage 4 (bypass and erosion).

After lobe aggradation and progradation, lobe may again be incised by the lobe channel (Bonnel et al., 2005). The progradation of lobe elements usually occurs by lobe "evitment" or "avoidance" (Turakiewicz, 2004; Jegou et al., 2008). When avulsion occurs, the channel quickly settles around the preceding lobe element and new lobe element forms downward. In this case, the channel emplacement occurs by topographic compensation (Mutti and Sonnino, 1981). In the Motta San Giovanni Formation, this topographic compensation is not always observed and the new bypass channel (Stage 3) is generally right on the top of the previous aggrading lobe axis or channel. Stage 3 cannot thus be considered a simple avulsion but rather a major milestone in the evolution of our studied intraslope lobe. An alternative interpretation would be that there was no space for the channel to avulse to a new low but was forced to stay more or less in the same position. Finally, the incisions/channels developed in the upstream CLTZ are not filled by the channel/levee facies during the back-filling stage, but by a new prograding lobe from the following cycle (new stage 1) suggesting that the hydraulic jump was very efficient in flushing sediment in the CLTZ before the next cycle.

Therefore, we speculate that this intraslope lobe system has a peculiarity, with a back-and-forth hydraulic jump dynamic. Hydraulic jump location could be described as normal jump when it occurs at the slope break (kinematic energy equals potential energy), flushed jump when occurring downstream of a slope break (kinematic > potential), or submerged jump when occurring upstream of the slope break (kinematic < potential) (Rajaratnam, 1967; Komar, 1971; Hager 1992; Cartigny et al., 2013). We propose that during Stage 1, the hydraulic jump was progressively flushed downstream the CLTZ. Then during Stage 2, it migrated upstream and stabilized in the CLTZ progressively evolving to submerged jump. The energy loss is maximal resulting in thick and massive packages of sandstones deposited all over the lobe area. Stage 3 finally recorded a renewal downstream migration with a normal jump emplacement, probably in response to the lowering of slope in the depositional lobe domain when compared to the upstream bypassed CLTZ. A new slope break marks the establishment of a normal hydraulic jump (Stage 3) following the previous submerged jump (Stage 2). Stage 4 is characterized by a rapid abandonment of the depositional system, which shares similarities with common lobe "evitment" or "avoidance." We thus propose that intraslope lobe from the Motta San Giovanni Formation is characterized by back-and-forth migration of the hydraulic jump from flushed, to submerged and finally normal jump.

CONCLUSION

We present a detailed characterization of some outcropping intraslope lobes of the Miocene Motta San Giovanni Formation (Calabria), which were deposited and perched within sub-basins, along a transform margin. The results can be summarized in two points:

1. Based on the analysis of facies associations and stratigraphic architecture, we propose a depositional model diagnostic of intraslope lobes in a complex slope setting. Four main stages of evolution were identified with, *1*) isolated detached lobe precursor during Stage 1, *2*) prograding and aggrading lobe elements associated with a relatively stable submerged hydraulic jump in the CLTZ during Stage 2, *3*) bypass associated with lateral accretion and local aggradation interpreted as a renewal of normal hydraulic jump emplacement, and *4*) rapid abandonment during Stage 4.

2. A comparison with well-known intraslope and confined lobes, as well as basin floor lobes, is proposed, highlighting that the intraslope lobes deposited along transform margin are particularly small and relatively thin sandy deposits. Lobe elements are ca. 100–500 m wide, 200–600 m long, and 2–7 m thick. Lobes are ca. 300–3000 m wide, 500–5000 m long, and 2–22 m thick. They could be considered end-member in a lobe classification based on their Net-to-Gross content and their thickness/width ratio, largely driven by flow stripping and overspill processes in such structurally confined basins.

DATA AVAILABILITY STATEMENT

The raw data supporting the conclusions of this article will be made available by the authors, without undue reservation.

AUTHOR CONTRIBUTIONS

SR, SB, JB, and PB contributed to conception and design of the study. SR organized the database and interpretation. JS acquired and built most of the 3D outcrop models. SR wrote the first draft of the manuscript. All authors contributed to manuscript revision, read, and approved the submitted version.

REFERENCES

Adeogba, A. A., McHargue, T. R., and Graham, S. A. (2005). Transient Fan Architecture and Depositional Controls from Near-Surface 3-D Seismic Data, Niger Delta Continental Slope. *Bulletin* 89, 627–643. doi:10.1306/11200404025

Albertão, G. A., Mulder, T., and Eschard, R. (2011). Impact of Salt-Related Palaeotopography on the Distribution of Turbidite Reservoirs: Evidence from Well-Seismic Analyses and Structural Restorations in the Brazilian Offshore. *Mar. Pet. Geology* 28, 1023–1046. doi:10.1016/j.marpetgeo.2010.09.009

Allen, J. R. L. (1971). Instantaneous Sediment Deposition Rates Deduced from Climbing-Ripple Cross-Lamination. *J. Geol. Soc.* 127, 553–561. doi:10.1144/gsl.jgs.1971.127.06.02

Allen, J. R. L. (1982). *Sedimentary Structures: Their Character and Physical Basis*. Amsterdam: Elsevier, 1, 593.

Arnott, R. W. C., and Al-Mufti, O. (2017). Deep-Marine Pseudo Dune Cross-Stratification-Similar, but Completely Different. *J. Sediment. Res.* 87, 312–323. doi:10.2110/jsr.2017.21

Arnott, R. W. C., and Hand, B. C. (1989). Bedforms, Primary Structures and Grain Fabric in the Presence of Suspended Sediment Rain. *J. Sediment. Pet.* 59, 1062–1069. doi:10.1306/212f90f2-2b24-11d7-8648000102c1865d

Barrier, P. (1987). Stratigraphie des dépots pliocènes et pleistocènes du Detroit de Messine (Italie). *Doc. Trav. Inst. Géol. Albert de Lapparent (Igal)* 11, 59–81.

Barrier, P., Casale, V., Costa, B., Di Geronimo, L., Olivieri, O., and Rosso, A. (1986). La sezione pliopleistocenica di Pavigliana (Reggio Calabria). *Boll. Soc. Pal. Ital.* 25 (2), 3–144.

Barrier, P., Di Geronimo, I., and Montenat, C. (1987). Le Détroit de Messine (Italie). Evolution tectono-sédimentaire récente (pliocène et quaternaire) et environnement actuel. *Doc. Trav. Inst. Géol. Albert de Lapparent (Igal)*, 11, 3.

Barrier, P. (1982). *Étude préliminaire des formations pliocènes et quaternaires du Sud de Reggio di Calabria (Italie) ; (tome I), Étude du Rione Branca (tome II)*. MS dissertation. Beauvais: M.A.G 3. Institut Géologique Albert-de-Lapparent IGAL.

Barton, M. D. (2012). "Evolution of an Intra-slope Apron, Offshore Niger delta Slope: Impact of Step Geometry on Apron Architecture," in *Application of the Principles of Seismic Geomorphology to Continental-Slope and Base-Of-Slope Systems: Case Studies from Seafloor and Near-Seafloor Analogues*. Editors B. E. Prather, M. E. Deptuck, D. Mohrig, B. van Hoorn, and R. B. Wynn (SEPM Special Publication), 99, 181–197. doi:10.2110/pec.12.99.0181

Becue, F. (1988). *Le Tortonien de Catanzaro (Calabre - Italie)*. Master's thesis. Beauvais: M.G. 25 Institut Géologique Albert-de-Lapparent IGAL.

Best, J., and Bridge, J. (1992). The Morphology and Dynamics of Low Amplitude Bedwaves upon Upper Stage Plane Beds and the Preservation of Planar Laminae. *Sedimentology* 39, 737–752. doi:10.1111/j.1365-3091.1992.tb02150.x

Bonardi, G., Cavazza, W., Perrone, V., and Rossi, S. (2001). "Calabria-Peloritani Terrane and Northern Ionian Sea," in *Anatomy of an Orogen: The Apennines and Adjacent Mediterranean Basins: Dordrecht, The Netherlands*. Editors G. B. Vai and I. P. Martini (Kluwer Academic Publishers), 287–306. doi:10.1007/978-94-015-9829-3_17

Bonardi, G., Giunta, G., Perrone, V., Russo, M., Zuppetta, A., and Ciampo, G. (1980). Osservazioni sull'evoluzione dell'Arco Calabro–peloritano nel Miocene inferiore: la Formazione di Stilo–Capo d'Orlando. *Bollettino Societa Geologica Italiana* 99, 365–393.

Bonnel, C., Dennielou, B., Droz, L., Mulder, T., and Berné, S. (2005). Architecture and Depositional Pattern of the Rhône Neofan and Recent Gravity Activity in the Gulf of Lions (Western Mediterranean). *Mar. Pet. Geology* 22 (6–7), 827–843. doi:10.1016/j.marpetgeo.2005.03.003

Booth, J. R., Dean, M. C., DuVernay, A. E., and Styzen, M. J. (2003). Paleo-bathymetric Controls on the Stratigraphic Architecture and Reservoir Development of Confined Fans in the Auger Basin: Central Gulf of Mexico Slope. *Mar. Pet. Geology* 20, 563–586. doi:10.1016/j.marpetgeo.2003.03.008

Bouchet, F. (1990). *Étude sédimentaire et structurale de la série oligo-miocène et plio-quaternaire de la région de Melito (Calabre - Italie)*. MS dissertation. Beauvais: M.A.G. 65 Institut Géologique Albert-de-Lapparent IGAL.

Boullin, J. P., Durand-Delga, M., and Olivier, P. (1986). "Betic Rifian and Tyrrhenian Arc: Distinctive Features, Genesis and Development Stages," in *The Origin of Arcs*. Editor F. Wezel (New York, NY: Elsevier), 281–304.

Bouma, A. H. (1962). *Sedimentology of Some Flysch Deposits: A Graphic Approach to Facies Interpretation*. Amsterdam: Elsevier, 168.

Bourel, M., and Degrave, C. (2020). *Étude des relations entre la tectonique régionale et les formations turbiditiques du Miocène de la formation de Motta San Giovanni, Calabre, Italie*. Beauvais: M.I.R. Institut Polytechnique UniLaSalle, 875, 112.

Brooks, H. L., Hodgson, D. M., Brunt, R. L., Peakall, J., Hofstra, M., and Flint, S. S. (2018). Deep-water Channel-Lobe Transition Zone Dynamics: Processes and Depositional Architecture, an Example from the Karoo Basin, South Africa. *GSA Bull.* 130, 1723–1746. doi:10.1130/B31714.1

Bruhn, C. H. L., Gomes, J. A. T., Del Lucchese, C., Jr., and Johann, P. R. S. (2003). Campos Basin: Reservoir Characterization and Management – Historical Overview and Future Challenges," in Offshore Technology Conference, Houston, TX, May 5–8, 2003. doi:10.4043/15220-MS

Brunt, R. L., Hodgson, D. M., Flint, S. S., Pringle, J. K., Di Celma, C., Prélat, A., et al. (2013). Confined to Unconfined: Anatomy of a Base of Slope Succession, Karoo

Basin, South Africa. *Mar. Pet. Geology* 41, 206–221. doi:10.1016/j.marpetgeo.2012.02.007

Brutto, F., Muto, F., Loreto, M. F., D'Amico, S., De Paola, N., Tripodi, V., et al. (2018). "Quaternary Stress Field and Faulting in the Western Part of the Catanzaro Trough (Calabria, Southern Italy)," in *Moment Tensor Solutions*. Editor S. D'Amico (Springer Natural Hazards), 619–642. doi:10.1007/978-3-319-77359-9_28

Burgreen, B., and Graham, S. (2014). Evolution of a Deep-Water Lobe System in the Neogene Trench-Slope Setting of the East Coast Basin, New Zealand: Lobe Stratigraphy and Architecture in a Weakly Confined basin Configuration. *Mar. Pet. Geology* 54, 1–22. doi:10.1016/j.marpetgeo.2014.02.011

Butler, R. W. H., Pinter, P. R., Maniscalco, R., and Hartley, A. J. (2020) Deep-water Sand-Fairway Mapping as a Tool for Tectonic Restoration: Decoding Miocene central Mediterranean Palaeogeography Using the Numidian Turbidites of Southern Italy. *J. Geol. Soc.* 177, 766–783. doi:10.1144/jgs2020-008

Cartigny, M. J. B., Eggenhuisen, J. T., Hansen, E. W. M., and Postma, G. (2013). Concentration Dependent Flow Stratification in Experimental High-Density Turbidity Currents and Their Relevance to Turbidite Facies Models. *J. Sediment. Res.* 83, 1046–1064. doi:10.2110/jsr.2013.71

Cavazza, W., Blenkinsop, J., DeCelles, P., Patterson, R. T., and Reinhardt, E. (1997). Stratigrafia e sedimentologia della sequenza sedimentaria Oligocenico-Quaternaria del Bacino Calabro-Ionico. *Boll. Soc. Geol. It.* 116, 51–77.

Cavazza, W., and Ingersoll, R. V. (2005). Detrital Modes of the Ionian Forearc Basin Fill (Oligocene-Quaternary) Reflect the Tectonic Evolution of the Calabria-Peloritani Terrane (Southern Italy). *J. Sediment. Res.* 75, 268–279. doi:10.2110/jsr.2005.020

Chirol, H., and Kubiak, T. (2019). *Etude de l'architecture des corps turbiditiques miocènes de la formation de Motta San Giovanni, Secteur Ouest, Calabre, Italie*. Beauvais: M.I.R. Institut Polytechnique UniLaSalle, 839, 60.

Colas, E., and Ripoll, A. (2017). *Etude sédimentologique et structurale de l'architecture des corps turbiditiques miocènes au niveau du village de Lazzaro*. Beauvais: M.I.R.Institut Polytechnique UniLaSalle, 839, 141.

Cortese, E. (1895). Descrizione Geologica Della Calabria. *Memorie descrittive Carta Geologica d'Italia* 9, 310.

Critelli, S., Muto, F., Perri, F., and Tripodi, V. (2017). Interpreting Provenance Relations from Sandstone Detrital Modes, Southern Italy Foreland Region: Stratigraphic Record of the Miocene Tectonic Evolution. *Mar. Pet. Geology* 87, 47–59. doi:10.1016/j.marpetgeo.2017.01.026

Critelli, S., Muto, F., Tripodi, V., and Perri, F. (2011). "Relationships between Lithospheric Flexure, Thrust Tectonics and Stratigraphic Sequences in Foreland Setting: the Southern Apennines Foreland basin System, Italy," in *New Frontiers in Tectonic Research at the Midst of Plate Convergence*. Editor U. Schattner (Rijeka, Croatia: Intech Open Access Publisher, Janeza Trdine), 9, 121–170. doi:10.5772/24120

Critelli, S. (2018). Provenance of Mesozoic to Cenozoic Circum-Mediterranean Sandstones in Relation to Tectonic Setting. *Earth-Science Rev.* 185, 624–648. doi:10.1016/j.earscirev.2018.07.001

Dennielou, B., Droz, L., Babonneau, N., Jacq, C., Bonnel, C., Picot, M., et al. (2017). Morphology, Structure, Composition and Build-Up Processes of the Active Channel-Mouth Lobe Complex of the Congo Deep-Sea Fan with Inputs from Remotely Operated Underwater Vehicle (ROV) Multibeam and Video Surveys. *Deep Sea Res. Part Topical Stud. Oceanography* 142, 25–49. doi:10.1016/j.dsr2.2017.03.010

Deptuck, M. E., Piper, D. J. W., Savoye, B., and Gervais, A. (2008). Dimensions and Architecture of Late Pleistocene Submarine Lobes off the Northern Margin of East Corsica. *Sedimentology* 55, 869–898. doi:10.1111/j.1365-3091.2007.00926.x

Dercourt, J., Zonenshain, L. P., Ricou, L.-E., Kazmin, V. G., Le Pichon, X., Knipper, A. L., et al. (1986). Geological Evolution of the Tethys belt from the Atlantic to the Pamirs since the Lias. *Tectonophysics* 123, 241–315. doi:10.1016/0040-1951(86)90199-x

Deschamps, R., Doligez, B., Schmitz, J., Joseph, P., Rohais, S., Pellerin, M., et al. (2017). De la reconstitution numérique 3D d'affleurements au modèle de réservoir : une approche intégrée. *Géologues*, 68–71.

Deschamps, R., Schmitz, J., Daniel, J-M., and Joseph, P. (2013). *Method for Exploiting a Subsurface deposit Comprising at Least One Geological Outcrop by Means of Photogrammetry*.

Dewey, J. F., Helman, M. L., Knott, S. D., Turco, E., and Hutton, D. H. W. (1989). "Kinematics of the Western Mediterranean," in *Alpine Tectonics*. Editors M. P. Coward, D. Dietrich, and R. G. Park (Geological Society, London, Special Publications), 45, 265–283. doi:10.1144/gsl.sp.1989.045.01.15

Eschard, R., Albouy, E., Gaumet, F., and Ayub, A. (2004). "Comparing the Depositional Architecture of basin Floor Fans and Slope Fans in the Pab Sandstone, Maastrichtian, Pakistan," in *Confined Turbidite Systems*. Editor S. A. Lomas (Geological Society of London, Special Publications), 222, 159–185. doi:10.1144/gsl.sp.2004.222.01.09

Etienne, S., Mulder, T., Bez, M., Desaubliaux, G., Kwasniewski, A., Parize, O., et al. (2012). Multiple Scale Characterization of Sand-Rich Distal Lobe deposit Variability: Examples from the Annot Sandstones Formation, Eocene-Oligocene, SE France. *Sediment. Geology* 273-274, 1–18. doi:10.1016/j.sedgeo.2012.05.003

Faccenna, C., Becker, T. W., Lucente, F. P., Jolivet, L., and Rossetti, F. (2001). History of Subduction and Back-Arc Extension in the Central Mediterranean. *Geophys. J. Int.* 145, 809–820. doi:10.1046/j.0956-540x.2001.01435.x

Ferry, J.-N., Mulder, T., Parize, O., and Raillard, S. (2005). "Concept of Equilibrium Profile in Deep-Water Turbidite System: Effects of Local Physiographic Changes on the Nature of Sedimentary Process and the Geometries of Deposits," in *Submarine Slope Systems: Processes and Products*. Editors D. M. Hodgson and S. S. Flint (Geological Society of London, Special Publications), 244, 181–193. doi:10.1144/gsl.sp.2005.244.01.11

Fiduk, J. C., Weimer, P., Trudgill, B. D., Rowan, M. G., Gale, P. E., Phair, R. L., et al. (1999). The Perdido Fold belt, Northwestern Deep Gulf of Mexico, Part 2: Seismic Stratigraphy and Petroleum Systems. *AAPG Bull.* 83, 578–612. doi:10.1306/00aa9c00-1730-11d7-8645000102c1865d

Flint, S. S., Hodgson, D. M., Sprague, A. R., Brunt, R. L., van der Merwe, W. C., Figueiredo, J., et al. (2011). Depositional Architecture and Sequence Stratigraphy of the Karoo Basin Floor to Shelf Edge Succession, Laingsburg Depocentre, South Africa. *Mar. Pet. Geology* 28, 658–674. doi:10.1016/j.marpetgeo.2010.06.008

Gaillot, G., Hoyal, D., Demko, T., and Abreu, V. (2015). *Building Blocks of the Modern Golo Submarine Fan: Insights from High-Resolution Seismic Data*. Krakow, Poland: 31st IAS Conference, 22–25.

Gallet de Saint-Aurin, J-M. (1988). *Approche tectono-sédimentaire du Bassin néogène et quaternaire d'Ardore-Siderno (Calabre, Italie)*. MS dissertation. Beauvais: M.A.G. 53 Institut Géologique Albert-de-Lapparent IGAL.

Gamberi, F., and Rovere, M. (2011). Architecture of a Modern Transient Slope Fan (Villafranca Fan, Gioia Basin-Southeastern Tyrrhenian Sea). *Sediment. Geology* 236, 211–225. doi:10.1016/j.sedgeo.2011.01.007

Gamberi, F., Rovere, M., and Marani, M. (2011). Mass-transport Complex Evolution in a Tectonically Active Margin (Gioia Basin, Southeastern Tyrrhenian Sea). *Mar. Geology* 279, 98–110. doi:10.1016/j.margeo.2010.10.015

Gervais, A., Savoye, B., Mulder, T., and Gonthier, E. (2006). Sandy Modern Turbidite Lobes: A New Insight from High Resolution Seismic Data. *Mar. Pet. Geology* 23, 485–502. doi:10.1016/j.marpetgeo.2005.10.006

Gervais, A., Savoye, B., Piper, D. J. W., Mulder, T., Cremer, M., and Pichevin, L. (2004). "Present Morphology and Depositional Architecture of a sandy Confined Submarine System: the Golo Turbidite System (Eastern Margin of Corsica)," in *Confined Turbidite Systems*. Editors S. A. Lomas and P. Joseph (Geological Society Special Publication), 222, 59–89. doi:10.1144/gsl.sp.2004.222.01.05

Groenenberg, R. M., Hodgson, D. M., Prélat, A., Luthi, S. M., and Flint, S. S. (2010). Flow-Deposit Interaction in Submarine Lobes: Insights from Outcrop Observations and Realizations of a Process-Based Numerical Model. *J. Sediment. Res.* 80, 252–267. doi:10.2110/jsr.2010.028

Guillet de Chatelus, F., and Prosperi, A. (2020). *Impact de l'activité syn-sédimentaire sur les architectures turbiditiques miocènes de Motta San Giovanni, Calabre – Italie*. Beauvais: M.I.R. Institut Polytechnique UniLaSalle, 889, 41.

Guillocheau, F., Quéméner, J.-M., Robin, C., Joseph, P., and Broucke, O. (2004). "Genetic Units/parasequences of the Annot Turbidite System, SE France," in *Deep Water Sedimentation in the Alpine Basin of SE France. New Perspectives on the Grès d'Annot and Related Systems*. Editors P. Joseph and S. A. Lomas (Geological Society, London, Special Publication), 221, 181–202. doi:10.1144/gsl.sp.2004.221.01.10

Guillois, M., and Polard-Taine, P. (2016). in *Etude sédimentologique et structurale de l'architecture des corps turbiditiques miocènes au niveau du village de Motta San Giovanni* Beauvais: Institut Polytechnique Lasalle Beauvais, 131.

Hager, W. L. (1992). *Energy Dissipators and Hydraulic Jumps*. Dordrecht: Kluwer Academic Publishers.

Haughton, P., Davis, C., McCaffrey, W., and Barker, S. (2009). Hybrid Sediment Gravity Flow Deposits - Classification, Origin and Significance. *Mar. Pet. Geology* 26, 1900–1918. doi:10.1016/j.marpetgeo.2009.02.012

Hodgson, D. M. (2009). Distribution and Origin of Hybrid Beds in Sand-Rich Submarine Fans of the Tanqua Depocentre, Karoo Basin, South Africa. *Mar. Pet. Geology* 26, 1940–1956. doi:10.1016/j.marpetgeo.2009.02.011

Hodgson, D. M., Kane, I. A., Flint, S. S., Brunt, R. L., and Ortiz-Karpf, A. (2016). Time-Transgressive Confinement on the Slope and the Progradation of Basin-Floor Fans: Implications for the Sequence Stratigraphy of Deep-Water Deposits. *J. Sediment. Res.* 86, 73–86. doi:10.2110/jsr.2016.3

Hofstra, M., Hodgson, D. M., Peakall, J., and Flint, S. S. (2015). Giant Scour-Fills in Ancient Channel-Lobe Transition Zones: Formative Processes and Depositional Architecture. *Sediment. Geology* 329, 98–114. doi:10.1016/j.sedgeo.2015.09.004

Holman, W. E., Robertson, S. S., Lawrence, D. T., and Rossen, C. (1994). "Field Development, Depositional Model, and Production Performance of the Turbiditic "J" Sands at Prospect Bullwinkle, Green Canyon 65 Field, Outer-Shelf Gulf of Mexico," in *Submarine Fans and Turbidite Systems—Sequence Stratigraphy, Reservoir Architecture, and Production Characteristics*. Editors P. Weimer, A. H. Bouma, and B. F. Perkins (GCSSEPM Fifteenth Annual Research Conference), 139–150. doi:10.5724/gcs.94.15.0139

Jegou, I., Savoye, B., Pirmez, C., and Droz, L. (2008). Channel-mouth Lobe Complex of the Recent Amazon Fan: The Missing Piece. *Mar. Geology* 252, 62–77. doi:10.1016/j.margeo.2008.03.004

Jobe, Z. R., Lowe, D. R., and Morris, W. R. (2012). Climbing-ripple Successions in Turbidite Systems: Depositional Environments, Sedimentation Rates and Accumulation Times. *Sedimentology* 59, 867–898. doi:10.1111/j.1365-3091.2011.01283.x

Jobe, Z. R., Sylvester, Z., Howes, N., Pirmez, C., Parker, A., Cantelli, A., et al. (2017). High-resolution, Millennial-Scale Patterns of Bed Compensation on a Sand-Rich Intraslope Submarine Fan, Western Niger Delta Slope. *Geol. Soc. America Bull.* 129, 23–37. doi:10.1130/b31440.1

Jolivet, L., Menant, A., Roche, V., Le Pourhiet, L., Maillard, A., Augier, R., et al. (2021). Transfer Zones in Mediterranean Back-Arc Regions and Tear Faults. *BSGF - Earth Sci. Bull.* 192, 11. doi:10.1051/bsgf/2021006

Joseph, P., Babonneau, N., Bourgeois, A., Cotteret, G., Eschard, R., Garin, B., et al. (2000). "The Annot Sandstone Outcrops (French Alps): Architecture Description as Input for Quantification and 3D Reservoir Modeling," in *Deep-Water Reservoirs of the World: Gulf Coast Section SEPM Foundation 20th Annual Research Conference*. Editor P. Weimer (SEPM Special Publication), 28, 422–449. doi:10.5724/gcs.00.15.0422

Joseph, P., and Lomas, S. A. (2004). "Deep-water Sedimentation in the Alpine Foreland Basin of SE France: New Perspectives on the Grès d'Annot and Related Systems-An Introduction," in *Eep-Water Sedimentation in the Alpine Basin of SE France: New Perspectives on the Grès d'Annot and Related Systems*. Editors P. Joseph and S. A. Lomas Geological Society, London, Special Publications, 221, 1–16. doi:10.1144/gsl.sp.2004.221.01.01

Kane, I. A., and Hodgson, D. M. (2011). Sedimentological Criteria to Differentiate Submarine Channel Levee Subenvironments: Exhumed Examples from the Rosario Fm. (Upper Cretaceous) of Baja California, Mexico, and the Fort Brown Fm. (Permian), Karoo Basin, S. Africa. *Mar. Pet. Geology* 28, 807–823. doi:10.1016/j.marpetgeo.2010.05.009

Kezirian, F., Barrier, P., Bouillin, J.-P., and Janin, M.-C. (1994). L'Oligo-Miocène péloritain (Sicile) : un témoin du rifting du Bassin algéro-provençal. *C. R. Acad. Sci. Paris, Série* 319, 699–704.

Kleverlaan, K. (1989). Three Distinctive Feeder-Lobe Systems within One Time Slice of the Tortonian Tabernas Fan, SE Spain. *Sedimentology* 36, 25–45. doi:10.1111/j.1365-3091.1989.tb00818.x

Kneller, B. C., and Branney, M. J. (1995). Sustained High-Density Turbidity Currents and the Deposition of Thick Massive Sands. *Sedimentology* 42, 607–616. doi:10.1111/j.1365-3091.1995.tb00395.x

Komar, P. D. (1971). Hydraulic Jumps in Turbidity Currents. *Geol. Soc. America Bull.* 82, 1477–1487. doi:10.1130/0016-7606(1971)82[1477:hjitc]2.0.co;2

Leclair, S. F., and Arnott, R. W. C. (2005). Parallel Lamination Formed by High-Density Turbidity Currents. *J. Sediment. Res.* 75, 1–5. doi:10.2110/jsr.2005.001

Leprêtre, R., Frizon de Lamotte, D., Déverchère, J., and Graindorge, D. (2019). Géodynamique de la Méditerranée occidentale : une série de bassins d'arrière-arc dans un environnement montagneux. *Géochronique* n149, 20–34.

Li, L., Wang, Y., Xu, Q., Zhao, J., and Li, D. (2012). Seismic Geomorphology and Main Controls of Deep-Water Gravity Flow Sedimentary Process on the Slope of the Northern South China Sea. *Sci. China Earth Sci.* 55, 747–757. doi:10.1007/s11430-012-4396-1

Lowe, D. R. (1982). Sediment Gravity Flows: II Depositional Models with Special Reference to the Deposits of High Density Turbidity Currents. *J. Sed. Res.* 52, 279–297. doi:10.1306/212f7f31-2b24-11d7-8648000102c1865d

MacGregor, D., Robinson, J., and Spear, G. (2003). *Play Fairways of the Gulf of Guinea Transform Margin*. London: Geological Society, Special Publications, 207, 131–150. doi:10.1144/GSL.SP.2003.207.7

Manoux, J. (1999). *Évolution tectono-sédimentaire de la partie ouest du Bassin de Melito di Porto Salvo au Miocène et au Plio-Quaternaire. (Calabre - Italie)*. MS dissertation. Beauvais: M.A.G. 211 Institut Géologique Albert-de-Lapparent IGAL, 103.

Marchès, E., Mulder, T., Gonthier, E., Cremer, M., Hanquiez, V., Garlan, T., et al. (2010). Perched Lobe Formation in the Gulf of Cadiz: Interactions Between Gravity Processes and Contour Currents (Algarve Margin, Southern Portugal). *Sediment. Geology* 229, 81–94. doi:10.1016/j.sedgeo.2009.03.008

Marchiel, A., and Rispal, N. (2019). *Etude de l'architecture des corps turbiditiques Miocène de la formation de Motta San Giovanni, Secteur Est, Calabre, Italie*. Beauvais: M.I.R. Institut Polytechnique UniLaSalle, 852, 110.

Marini, M., Patacci, M., Felletti, F., and McCaffrey, W. D. (2016). Fill to Spill Stratigraphic Evolution of a Confined Turbidite Mini-basin Succession, and its Likely Well Bore Expression: The Castagnola Fm, NW Italy. *Mar. Pet. Geology* 69, 94–111. doi:10.1016/j.marpetgeo.2015.10.014

McArthur, A. D., Bailleul, J., Mahieux, G., Claussmann, B., Wunderlich, A., and McCaffrey, W. D. (2021). Deformation-sedimentation Feedback and the Development of Anomalously Thick Aggradational Turbidite Lobes: Outcrop and Subsurface Examples from the Hikurangi Margin, New Zealand. *J. Sediment. Res.* 91 (4), 362–389. doi:10.2110/jsr.2020.013

McGee, D. T., Bilinski, P. W., Gary, P. S., Pfeiffer, D. S., Sheiman, J. L., Lawrence, D. T., et al. (1994). "Geologic Models and Reservoir Geometries of Auger Field, deepwater Gulf of Mexico," in *Submarine Fans and Turbidite Systems-Sequence Stratigraphy, Reservoir Architecture, and Production Characteristics*. Editors P. Weimer, A. H. Bouma, and B. F. Perkins (GCSSEPM Fifteenth Annual Research Conference), 245–256. doi:10.5724/gcs.94.15.0245

Milia, A., Iannace, P., and Torrente, M. M. (2021). The Meeting Place of Backarc and Foreland Rifting: The Example of the Offshore Western Sicily (Central Mediterranean). *Glob. Planet. Change* 198, 103408. doi:10.1016/j.gloplacha.2020.103408

Moraes, M. A. S., Blaskovski, P. R., and Joseph, P. (2004). "The Grès d'Annot as an Analogue for Brazilian Cretaceous sandstone Reservoirs: Comparing Convergent to Passive-Margin Confined Turbidites," in *Deep-Water Sedimentation in the Alpine Basin of SE France: New Perspectives on the Grès d'Annot and Related Systems*. Editors P. Joseph and S. A. Lomas (Geological Society, London, Special Publications), 221, 419–437. doi:10.1144/gsl.sp.2004.221.01.23

Morlo, T. (1985). *Étude préliminaire des formations tortoniennes à pléistocènes du Bassin de Mesima (Italie)*. MS dissertation. Beauvais: M.A.G. 27 Institut Géologique Albert-de-Lapparent IGAL.

Mulder, T., Callec, Y., Parize, O., Joseph, P., Schneider, J.-L., Robin, C., et al. (2010). High-resolution Analysis of Submarine Lobes Deposits: Seismic-Scale Outcrops of the Lauzanier Area (SE Alps, France). *Sediment. Geology* 229, 160–191. doi:10.1016/j.sedgeo.2009.11.005

Mulder, T., and Etienne, S. (2010). Lobes in Deep-Sea Turbidite Systems: State of the Art. *Sediment. Geology* 229, 75–80. doi:10.1016/j.sedgeo.2010.06.011

Mutti, E. (1992). *Turbidite Sandstones*. Milan, Italy: Agip-Instituto di Geologia. Università di Parma, 275.

Mutti, E., and Normark, W. R. (1987). "Comparing Examples of Modern and Ancient Turbidite Systems: Problems and Concepts," in *Marine Clastic Sedimentology: Concepts and Case Studies*. Editors J. K. Legget and G. G. Zuffa (London: Graham and Troutman). doi:10.1007/978-94-009-3241-8_1

Mutti, E., and Sonnino, M. (1981). *Compensation Cycles: A Diagnostic Feature of Turbidite sandstone Lobes. Int. Ass. Sediment*. Bologna, Italy: 2nd European Reg. Meet., 120–123.

Nicolleau, P., Vadet, A., Barrier, P., Bailleul, J., Brocheray, S., Kezirian, F., et al. *About the Serravalian Cidaris with Fan-Shaped Spines from Motta San Giovani (Calabria, Italy)*. Brest: Carnets de Géologie.

Ogniben, L. (1969). Schema introduttivo alla geologia del confi ne calabro-lucano. *Memorie della Societa Geologica Italiana* 8, 453–763.

Oluboyo, A. P., Gawthorpe, R. L., Bakke, K., and Hadler-Jacobsen, F. (2014). Salt Tectonic Controls on Deep-Water Turbidite Depositional Systems: Miocene, Southwestern Lower Congo Basin, Offshore Angola. *Basin Res.* 26, 597–620. doi:10.1111/bre.12051

Patterson, R. T., Blenkinsop, J., and Cavazza, W. (1995). Planktic Foraminiferal Biostratigraphy and 87Sr/86Sr Isotopic Stratigraphy of the Oligocene-To-Pleistocene Sedimentary Sequence in the Southeastern Calabrian Microplate, Southern Italy. *J. Paleontol.* 69, 7–20. doi:10.1017/s0022336000026871

Pellegrini, B. d. S., and Ribeiro, H. J. P. S. (2018). Exploratory Plays of Pará-Maranhão and Barreirinhas Basins in Deep and Ultra-deep Waters, Brazilian Equatorial Margin. *Braz. J. Geol.* 48 (3), 485–502. doi:10.1590/2317-4889201820180146

Pichancourt, T., and Terrier, J. (2016). *Etude du potentiel réservoir des corps turbiditiques Miocènes à proximité du village de Motta San Giovanni*. Beauvais: M.I.R. Institut Polytechnique UniLaSalle, 747, 83.

Pickering, K. T., and Clark, J. D. (1996). Architectural Elements and Growth Patterns of Submarine Channels: Application to Hydrocarbon Exploration. *Am. Assoc. Pet. Geologists Bull.* 80 (2), 194–221. doi:10.1306/64ed878c-1724-11d7-8645000102c1865d

Picot, M., Droz, L., Marsset, T., Dennielou, B., and Bez, M. (2016). Controls on Turbidite Sedimentation: Insights from a Quantitative Approach of Submarine Channel and Lobe Architecture (Late Quaternary Congo Fan). *Mar. Pet. Geology* 72, 423–446. doi:10.1016/j.marpetgeo.2016.02.004

Pirmez, C., Beaubouef, R. T., Friedmann, S. J., and Mohrig, D. C. (2000). "Equilibrium Profile and Baselevel in Submarine Channels: Examples from Late Pleistocene Systems and Implications for the Architecture of Deepwater Reservoirs," in *Deep-Water Reservoirs of the World: 20th Annual Research Conference, Gulf Coast Section Society of Economic Paleontologists and Mineralogists*. Editor P. Weimer, 782–805. doi:10.5724/gcs.00.15.0782

Plink-Björklund, P., and Steel, R. (2002). Sea-level Fall Below the Shelf Edge, Without Basin-floor Fans. *Geol.* 30, 115–118. doi:10.1130/0091-7613(2002)030<0115:slfbts>2.0.co;2

Postma, G., and Cartigny, M. J. B. (2014). Supercritical and Subcritical Turbidity Currents and Their Deposits–A Synthesis. *Geology* 42, 987–990. doi:10.1130/g35957.1

Postma, G., and Kleverlaan, K. (2018). Supercritical Flows and Their Control on the Architecture and Facies of Small-Radius Sand-Rich Fan Lobes. *Sediment. Geology* 364, 53–70. doi:10.1016/j.sedgeo.2017.11.015

Prather, B. E., Booth, J. R., Steffens, G. S., and Craig, P. A. (1998). Classification, Lithologic Calibration, and Stratigraphic Succession of Seismic Facies of Intraslope Basins Deep Water Gulf of Mexico, U.S.A. *AAPG Bull.* 82, 701–728.

Prather, B. E. (2003). Controls on Reservoir Distribution, Architecture and Stratigraphic Trapping in Slope Settings. *Mar. Pet. Geology* 20, 529–545. doi:10.1016/j.marpetgeo.2003.03.009

Prather, B. E., Pirmez, C., and Winker, C. D. (2012). "Stratigraphy of Linked Intraslope Basins: Brazos-Trinity System Western Gulf of Mexico," in *Case Studies from Seafloor and Near-Seafloor Analogues* (SEPM, Special Publication), 99, 83–109. doi:10.2110/pec.12.99.0083

Prélat, A., Covault, J. A., Hodgson, D. M., Fildani, A., and Flint, S. S. (2010). Intrinsic Controls on the Range of Volumes, Morphologies, and Dimensions of Submarine Lobes. *Sediment. Geology* 232, 658–674. doi:10.1016/j.sedgeo.2010.09.010

Prélat, A., Hodgson, D. M., and Flint, S. S. (2009). Evolution, Architecture and Hierarchy of Distributary Deep-Water Deposits: A High-Resolution Outcrop Investigation from the Permian Karoo Basin, South Africa. *Sedimentology* 56, 2132–2154. doi:10.1111/j.1365-3091.2009.01073.x

Pyles, D. R., Strachan, L. J., and Jennette, D. C. (2014). Lateral Juxtapositions of Channel and Lobe Elements in Distributive Submarine Fans: Three-Dimensional Outcrop Study of the Ross Sandstone and Geometric Model. *Geosphere* 10, 1104–1122. doi:10.1130/GES01042.1

Raber, C. (2003). *Synthèse géologique de la province de Reggio di Calabria. A 1/100 000e : carte et notice (Calabre, Italie)*. Master's thesis. Beauvais: M.I.G. 191 Institut Géologique Albert-de-Lapparent IGAL, 180.

Rajaratnam, N. (1967). Hydraulic Jumps. *Adv. Hydrosci.* 4, 197–280. doi:10.1016/b978-1-4831-9935-1.50011-2

Roda, C. (1965). *II calcare portlandiano a Dasycladacee di M. Mutolo*. Reggio Calabria: Geologica Romana 4, 259–290.

Rohais, S. (2000). *Évolution tectono-sédimentaire au Miocène et au Plio-Quaternaire du bassin de Palizzi à Brancaleone (Calabre, Italie)*. MS dissertation. Beauvais: M.A.G. 234 Institut Géologique Albert-de-Lapparent IGAL, 91.

Romagny, A., Jolivet, L., Menant, A., Bessière, E., Maillard, A., Canva, A., et al. (2020). Detailed Tectonic Reconstructions of the Western Mediterranean Region for the Last 35 Ma, Insights on Driving Mechanisms. *BSGF - Earth Sci. Bull.* 191, 37. doi:10.1051/bsgf/2020040

Russell B. Wynn,1 Neil H. Kenyon,2, R., Kenyon, N. H., Masson, D., Stow, D., and Weaver, P. (2002). Characterization and Recognition of Deep-Water Channel-Lobe Transition Zones. *Bulletin* 86, 1441–1462. doi:10.1306/61EEDCC4-173E-11D7-8645000102C1865D

Schepers, K. (1999). *Évolution tectono-sédimentaire de la partie Est du bassin de Melito di Porto Salvo au Miocène et au Plio-Quaternaire. (Calabre - Italie du Sud)*. Beauvais: M.A.G. Institut Géologique Albert-de-Lapparent IGAL, 217, 108.

Schmitz, J., Deschamps, R., Joseph, P., Lerat, O., Doligez, B., and Jardin, A. (2014). "From 3D Photogrammetric Outcrop Models to Reservoir Models: An Integrated Modelling Workflow," in *Presented at the Vertical Geology Conference* (LausanneSwitzerland, 5–7.

Selli, R. (1979). "Geologica e sismotettonica dello stretto di Messina," in *"L'attraversamento dello stretto de Messina e la sua fattibilita". Roma, 1978* Roma: Acad. Naz. Dei Lincei, 119–154.

Sinclair, H. D., and Tomasso, M. (2002). Depositional Evolution of Confined Turbidite Basins. *J. Sediment. Res.* 72, 451–456. doi:10.1306/111501720451

Southard, J. B. (1991). Experimental Determination of Bed-form Stability. *Annu. Rev. Earth Planet. Sci.* 19, 423–455. doi:10.1146/annurev.ea.19.050191.002231

Spychala, Y. T., Hodgson, D. M., Flint, S. S., and Mountney, N. P. (2015). Constraining the Sedimentology and Stratigraphy of Submarine Intraslope Lobe Deposits Using Exhumed Examples from the Karoo Basin, South Africa. *Sediment. Geology* 322, 67–81. doi:10.1016/j.sedgeo.2015.03.013

Spychala, Y. T., Hodgson, D. M., and Lee, D. R. (2017). Autogenic Controls on Hybrid Bed Distribution in Submarine Lobe Complexes. *Mar. Pet. Geology* 88, 1078–1093. doi:10.1016/j.marpetgeo.2017.09.005

Stow, D. A. V., and Piper, D. J. W. (1984). "Deep-water fine-grained Sediments: Facies Models," in *Fine-grained Sediments: Deep-Water Processes and Facies*. Editors D. A. V. Stow and D. J. W. Piper (Geological Society of London, Special Publication), 15, 611–646. doi:10.1144/gsl.sp.1984.015.01.38

Straub, K. M., and Pyles, D. R. (2012). Quantifying the Hierarchical Organization of Compensation in Submarine Fans Using Surface Statistics. *J. Sediment. Res.* 82, 889–898. doi:10.2110/jsr.2012.73

Talling, P. J. (2013). Hybrid Submarine Flows Comprising Turbidity Current and Cohesive Debris Flow: Deposits, Theoretical and Experimental Analyses, and Generalized Models. *Geosphere* 9, 460–488. doi:10.1130/ges00793.1

Talling, P. J., Masson, D. G., Sumner, E. J., and Malgesini, G. (2012). Subaqueous Sediment Density Flows: Depositional Processes and Deposit Types. *Sedimentology* 59, 1937–2003. doi:10.1111/j.1365-3091.2012.01353.x

Thomaïdis, C. (2000). *Évolution tectono-sédimentaire du bassin de Bova au Miocène et au Plio-Quaternaire (Calabre, Italie)*. MS dissertation. Beauvais: M.A.G. 237 Institut Géologique Albert-de-Lapparent IGAL, 93.

Tortorici, L., Monaco, C., Tansi, C., and Cocina, O. (1995). Recent and Active Tectonics in the Calabrian Arc (Southern Italy). *Tectonophysics* 243, 37–55. doi:10.1016/0040-1951(94)00190-K

Tripodi, V., Muto, F., Brutto, F., Perri, F., and Critelli, S. (2018). Neogene-Quaternary Evolution of the Forearc and Backarc Regions Between the Serre and Aspromonte Massifs, Calabria (Southern Italy). *Mar. Pet. Geology* 95, 328–343. doi:10.1016/j.marpetgeo.2018.03.028

Tripodi, V., Muto, F., and Critelli, S. (2013). Structural Style and Tectono-Stratigraphic Evolution of the Neogene-Quaternary Siderno Basin, Southern Calabrian Arc, Italy. *Int. Geology Rev.* 55, 468–481. doi:10.1080/00206814.2012.723859

Turakiewicz, G. (2004). *Mécanismes forçants dans les éventails turbiditiques des marges matures: exemple de l'éventail quaternaire du Congo*. Montpellier: Unpubl. Ph.D. Thesis, Univ. Montpellier II, 367.

Vallee, A. (2003). *Etude géologique du Monte Lepericchio : géométrie des corps sédimentaires et analyse des dépôts (Pellaro, Calabre - Italie)*. 307, Beauvais: M.A.G. Institut Géologique Albert-de-Lapparent IGAL, 57.

Vitale, S., and Ciarcia, S. (2013). Tectono-stratigraphic and Kinematic Evolution of the Southern Apennines/Calabria-Peloritani Terrane System (Italy). *Tectonophysics* 583, 164–182. doi:10.1016/j.tecto.2012.11.004

Walker, R. G. (1978). Deep-water Sandstone Facies and Ancient Submarine Fans: Models for Exploration of Stratigraphic Traps. *Bull. Am. Assoc. Pet. Geologists* 62, 932–966. doi:10.1306/c1ea4f77-16c9-11d7-8645000102c1865d

Wilson, J. T. (1965). A New Class of Faults and Their Bearing on continental Drift. *Nature* 207, 343–347. doi:10.1038/207343a0

Zhang, J.-J., Wu, S.-H., Fan, T.-E., Fan, H.-J., Jiang, L., Chen, C., et al. (2016). Research on the Architecture of Submarine-Fan Lobes in the Niger Delta Basin, Offshore West Africa. *J. Palaeogeogr.* 5, 185–204. doi:10.1016/j.jop.2016.05.005

Conflict of Interest: The authors declare that the research was conducted in the absence of any commercial or financial relationships that could be construed as a potential conflict of interest.